Mon. Not. R. Astron. Soc. **325,** 1081–1096 (2001)

Near-infrared spectroscopy of starburst galaxies

R. Coziol,[1,2★] R. Doyon[3] and S. Demers[3]

[1]*El Departamento de Astronomia de la Universidad de Guanajuato, Apartado Postal #144, 36000 Guanajuato, Gto México*
[2]*Observatoire de Besançon, UPRES–A 6091, B.P. 1615, F–25010 Besançon Cedex, France*
[3]*Département de Physique, Observatoire du Mont Mégantic, Université de Montréal, Montréal, Québec H3C 3J7, Canada*

Accepted 2001 March 16. Received 2001 March 16; in original form 2000 June 16

ABSTRACT

We present new *K*-band spectroscopy for a sample of 48 starburst galaxies, obtained using UKIRT in Hawaii. This constitutes a fair sample of the most common types of starburst galaxies found in the nearby Universe, containing galaxies with different morphologies, masses and metallicities, with far-infrared luminosity $L_{IR} < 10^{10}\,L_{\odot}$. The variety of near-infrared spectral features shown by these galaxies implies different bursts characteristics, which suggests that we survey galaxies with different star formation histories or at different stages of their burst evolution.

Using synthetic starburst models, we conclude that the ensemble of parameters that best describes starburst galaxies in the nearby Universe is a constant rate of star formation, a Salpeter initial mass function (IMF) with an upper mass cut-off of $M_{up} = 30\,M_{\odot}$ and bursts ages between 10 Myr and 1 Gyr. The model is fully consistent with the differences observed in the optical and far-infrared (FIR) between the different types of starbursts. It suggests that H II galaxies have younger bursts and lower metallicities than starburst nucleus galaxies (SBNGs), while luminous infrared galaxies (LIRGs) have younger bursts but higher metallicities.

Although the above solution from the synthetic starburst model is fully consistent with our data, it may not constitute a strong constraint on the duration of the bursts and the IMF. A possible alternative may be a sequence of short bursts (which may follow an universal IMF) over a relatively long period of time. In favour of the multiple-burst hypothesis, we distinguish in our spectra some variations of near-infrared (NIR) features with the aperture that can be interpreted as evidence that the burst regions are not homogeneous in space and time. We also found that the burst stellar populations are dominated by early-type B stars, a characteristic which seems difficult to explain with only one evolved burst.

Our observations suggest that the starburst phenomenon must be a sustained or self-sustained phenomenon: either star formation is continuous in time, or multiple bursts happen in sequence over a relatively long period of time. The generality of our observations implies that this is a characteristic of starburst galaxies in the nearby Universe.

Key words: galaxies: starburst – infrared: galaxies.

1 INTRODUCTION

Although a wealth of information has been accumulated on starburst galaxies over the last 30 yr, there are still fundamental questions that are left unanswered. In particular, we do not know if starburst galaxies form stars according to a universal Salpeter's initial mass function (IMF), as seems to be the case in normal galaxies (Elmegreen 1999), or if their IMF slope is flat or has a high lower mass cut-off, which would allow starburst galaxies to form preferentially massive stars (Rieke et al. 1993). Neither do we know if the typical duration of a burst is short, comparable to dynamical time-scales (Mas-Hesse & Kunth 1999), or if bursts are spread over a longer period of time (Meurer 2000).

In the past, various observations were carried out in order to find an answer to these two questions. Some of these studies have yielded quite surprising results. By comparing different luminosity ratios in the optical and far-infrared (FIR), Coziol (1996) found that most starburst galaxies may have kept forming stars at near constant rates over the last few billion years. The same conclusion was reached by Goldader et al. (1997b) for a sample of luminous

★E-mail: rcoziol@astro.ugto.mx

infrared galaxies ($L_{IR} > 10^{10}\,L_{\odot}$). Using synthetic starburst models, these authors found continuous star formation and burst ages varying between 10^7 and 10^9 yr. They also found that the best-fitted IMF is Salpeter like, but has an upper mass cut-off $M_{up} = 30\,M_{\odot}$. This kind of IMF in starburst galaxies was previously reported by Doyon, Puxley & Joseph (1992), which also suggest that the upper mass cut-off may vary from galaxy to galaxy.

Using different arguments based on various luminosity ratios, Deutsch & Willner (1986), Coziol & Demers (1995) and Coziol (1996) have found that B-type stars may be predominant in the ionized regions of massive starburst galaxies. Taken at face value, this last phenomenon seems consistent with the ages of bursts deduced by Goldader et al. (1997b) and the special form of the IMF found by these authors and Doyon et al. (1992). However, as was pointed out by Coziol 1996, assuming that starburst is a self-sustained phenomenon, this observation could also be interpreted in terms of a sequence of short bursts spread over a period of a few Gyr.

Evidence of extended or multiple bursts was recently found in many well-known active star-forming galaxies, like NGC 6764 (Schinnerer, Eckart & Boller 2000), Arp 220 (Anantharamaiah et al. 2000), NGC 1614 (Alonso-Herrero et al. 2000) and most recently M82 (de Grijs, O'Connell & Gallagher 2000). In another recent paper, Meurer (2000), using the *Hubble Space Telescope* (*HST*), distinguished different star clusters embedded in a diffuse glow of recently formed stars in nearby starburst galaxies. Examining their colours, he concluded that these clusters are consistent with instantaneous bursts with very young ages (from 0 up to 100 Myr), while the diffuse light seems to be produced by stars formed continuously over a period that is 10 times longer than the crossing times. A recent study of clusters in the irregular starburst galaxy NGC 1569 reveals similar clusters with ages between 3 Myr and 1 Gyr (Hunter et al. 2000). Old (3-Gyr) merger remnants were recently reported in the radio galaxy NGC 1316 (Goudfrooij et al. 2000). Multiple bursts and a low upper mass cut-off for the IMF may also be necessary to explain the number of different Wolf–Rayet sub-types in some WR galaxies (Schaerer et al. 2000). Even the small-mass and less evolved H II galaxies seem to be formed of age-composite stellar systems (Raimann et al. 2000).

In the present article, we explore these issues further by studying the spectral characteristics in the near infrared (NIR) of a new sample of 48 starburst galaxies with different physical characteristics. As it is well known, the starburst family is composed of a great variety of galaxy types, spanning several orders in size, mass, luminosity and gas metallicity (Salzer, MacAlpine & Boroson 1989). The burst characteristics of these galaxies may not necessarily be the same. By selecting galaxies with different physical characteristics, we therefore expect to draw a more general picture of the starburst phenomenon.

Our observations complete the study of luminous infrared galaxies (LIRGs) made by Goldader et al. (1995, 1997a,b). By adding these two samples together, one can compare starburst galaxies which span a factor of 100 in B and almost 1000 in FIR luminosity.

All the galaxies in our sample have modest FIR luminosity ($L_{IR} < 10^{10}\,L_{\odot}$). According to the *IRAS* luminosity function (Rieke & Lebofsky 1986; Vader & Simon 1987; Saunders et al. 1990), such galaxies may form the bulk of the star-forming galaxies in the nearby Universe. Our study, therefore, should reveal the 'normal' behaviour in the NIR of starburst galaxies in the nearby Universe.

The *K*-band window in the NIR is ideal for our study. The extinction caused by dust in this part of the spectrum is $\sim 1/10$ times that in the optical, which allows the comparison of star formation in galaxies with very different dust contents. The *K*-band window also offers several diagnostic spectral lines for studying young stellar populations: the narrow emission line Brγ provides some constraints on the relative number of O and B stars, while the CO band absorption, longward of 2.3 μm, can be used to estimate the ratio of red giants (RGs) over red super-giants (RSGs) and better constrain the duration and age of the bursts (Doyon, Joseph & Wright 1994). All these parameters can now be easily deduced from the available synthetic starburst models (Leitherer et al. 1999).

2 PRESENTATION OF THE SAMPLE

2.1 Selection criteria and biases

The 48 galaxies in our sample were selected using optical criteria: they present an ultraviolet (UV) excess in spectral lines or in the continuum; this is established using an objective prism or the multiple filters technique. The galaxies were taken from various sources: the Montreal Blue Galaxy (MBG) survey (Coziol et al. 1993; 1994), the sample of compact Kiso galaxies observed by Augarde et al. (1994), the University of Michigan survey (Salzer et al. 1989) and the spectrophotometric catalogue of H II galaxies (Terlevich et al. 1991).

Discussion of the biases affecting these various surveys can be found in Coziol et al. (1997). In principle, by adding galaxies from objective prism and multiple filters surveys one can span the complete spectrum of starburst galaxies, including H II galaxies and starburst nucleus galaxies (SBNGs). In practice, however, observation of H II galaxies in the NIR is more difficult: being less luminous than the SBNGs, the H II galaxies need too long exposure times. This explain the bias towards SBNGs in our sample.

By choosing galaxies which were selected based on optical criteria, we also favour galaxies which have a moderate to low FIR luminosity (Coziol et al. 1997). As we already mentioned in our introduction, this bias is opportune, as it allows us to study the most common type of starburst galaxies found in the nearby Universe (Rieke & Lebofsky 1986; Vader & Simon 1987; Saunders et al. 1990).

2.2 Physical characteristics

The physical characteristics of the galaxies in our sample are listed in Table 1. The redshifts, *B* magnitudes, morphologies and projected dimensions in the optical were all taken from the NASA/IPAC Extragalactic data base (NED). The distances, in column 3, were estimated assuming $H_0 = 75\,km\,s^{-1}\,Mpc^{-1}$, after correcting for the motion of the Sun. These distances were used to determine the linear scale in kpc, subtended in each galaxy by an angle of 1 arcmin on the sky (column 7). In many cases the morphology was not given. An examination of their images, as available in NED, allows us to determine that they look compact in appearance. These cases are identified in column 5. Only one galaxy, MBG 23388−1514, was not morphologically classified. Although we did not judge it as compact, we could not establish its morphology.

Various spectroscopic data were collected from the literature to complement our analysis. Optical spectra of these galaxies were obtained using comparable apertures (2–3 arcsec) and

Table 1. Characteristics of the sample.

Name	cz (km s^{-1})	D (Mpc)	B	Morph.	Dim. (arc−min)	l′ (kpc)	f(Hα) (erg s^{-1})	O/H	Act. Type	ref.
MBG 00027−1645	7339	99	13.8	Scd pec	1.4×0.5	29	…	…	…	…
MBG 00439−1342	675	10	13.8	S0 pec	1.3×1.2	3	38.23	−3.5	SBNG	(2b)
MBG 00461−1259	6407	86	13.5	(R)SB0 pec	0.9×0.6	25	41.05	−3.7	H II	(2a)
UM 306	5096	70	…	compact	<0.5	20	…	−3.8	H II	(3)
Mrk 1002	3168	44	13.3	S0	1.3×1.2	13	…	−3.1	SBNG	(8)
UM 372	12000	162	…	compact	<0.5	47	…	−3.9	H II	(3)
Mrk 363	2950	42	14.3	S0 pec	3.8×2.5	12	40.38	−3.5	…	(4)
MBG 02072−1022	3859	53	13.6	SA(r)0 pec	1.1×0.9	15	…	−3.4	SBNG	(2a)
MBG 02141−1134	4009	55	13.0	Sc pec	1.6×1.3	16	40.53	−3.1	SBNG	(2a)
Mrk 1055	10830	146	15.0	compact	0.2×0.2	42	…	…	…	…
Mrk 602	849	13	13.9	SB(rs)bc	1.2×0.9	4	40.52	…	…	(4)
KUG 0305−009	5860	80	15.2	compact	0.3×0.2	23	…	−3.2	SBNG	(1)
Mrk 603	2452	34	13.1	S0 pec	1.1×0.9	10	…	−3.6	SBNG	(9)
KUV 03073−0035	7080	96	17.0	compact	<0.5	28	…	−3.7	H II	(1)
MBG 03084−1059	5003	68	14.5	compact	0.5×0.5	20	40.12	−3.0	SBNG	(2b)
MBG 03183−1853	3949	53	14.1	SB(r)b	2.2×0.4	16	…	…	…	…
MBG 03317−2027	1233	17	13.5	S0 pec	1.2×1.1	5	…	…	…	…
KUG 0338+032	6615	90	16.5	compact	0.2×0.1	26	…	−3.7	H II	(1)
MBG 03468−2217	4193	56	13.8	(R)SB(l)a	1.0×0.6	16	40.92	−3.0	SBNG	(2a)
MBG 03523−2034	1733	24	14.4	SA0	1.0×0.7	7	…	−3.2	SBNG	(2a)
IRAS 04493−0553	2751	38	13.5	Sb pec	1.3×1.1	11	…	…	…	…
Mrk 1089	4068	56	13.3	SB(s)m pec/int	0.6×0.2	16	…	−3.5	SBNG	(10)
Mrk 1194	4470	61	13.4	SB0	1.7×1.2	18	41.09	…	…	(4)
II ZW 40	789	12	15.5	Sbc	0.6×0.2	4	38.95	−4.0	H II	(5)
KUG 0720+335	4028	56	…	Sp?/int?	<1.0	16	…	−3.0	SBNG	(1)
Mrk 384	4702	65	13.8	SBb	1.4×0.9	19	40.84	…	…	(4)
KUG 0815+249	2036	29	15.3	compact	0.2×0.2	9	…	−3.3	SBNG	(1)
KUG 0815+246	2435	35	15.3	compact	0.3×0.2	10	…	−3.7	…	(1)
KUG 0821+229	7553	103	15.6	compact	0.3×0.2	30	…	−3.6	SBNG	(1)
KUG 0825+252	2093	30	14.9	pec/int?	0.7×0.6	9	…	…	…	…
Mrk 90	4279	60	14.1	compact	0.7×0.6	17	40.52	…	…	(4)
Mrk 102	4269	60	14.5	compact	0.6×0.6	17	40.27	−3.7	…	(4)
Mrk 401	1699	25	13.6	(R)SB0/a	1.1×1.0	7	40.08	…	…	(4)
I ZW 18	742	13	15.6	Compact	<0.5	4	…	−3.5	H II	(6)
Mrk 404	1266	19	12.0	SAB(r)bc	2.9×1.6	6	…	…	…	…
Mrk 710	1494	22	13.0	SB(r)ab	2.2×1.4	6	…	…	…	…
Mrk 33	1461	22	13.4	Im pec	1.0×0.9	6	…	…	…	…
MBG 21513−1623	11190	149	15.3	S0/int?	0.2×0.2	43	41.41	−3.3	SBNG	(2a)
Mrk 307	5553	72	13.6	SBc pec	1.1×0.9	21	40.73	−3.1	…	(4)
MBG 22537−1650	3271	43	14.5	Sab	0.8×0.3	13	40.20	−3.4	SBNG	(2a)
KUG 2254+124	7629	100	…	compact	<0.5	29	…	…	SBNG	(1)
KUG 2300+163	2081	26	14.2	E3 pec	0.9×0.6	8	…	−3.7	H II	(1)
Mrk 326	3554	46	13.9	SAB(r)bc	1.6×1.0	13	40.52	…	SBNG	(4)
MBG 23318−1156	6180	82	14.5	pec	0.8×0.6	24	…	…	…	…
Mrk 538	2798	36	13.0	SB(s)b pec/int?	1.9×1.4	11	…	−3.6	SBNG	(4)
MBG 23372−1205	6429	85	…	pec	1.0×0.9	25	40.52	−3.5	SBNG	(2b)
MBG 23388−1514	9090	121	13.7	…	1.4×1.3	35	39.40	−3.8	H II	(2b)
Mrk 332	2406	30	13.0	SBc	1.4×1.3	9	…	…	…	…

Notes: (1) Augarde et al. 1994; (2a) Coziol et al. 1993; (2b) Coziol et al. 1994; (3) Salzer, MacAlpine & Boroson 1989; (4) Balzano 1983; (5) Masegosa, Moles & Campos-Aguilar 1994; (6) Izotov, Thuan & Lipovetsky 1998; (7) Kim et al. 1995; (8) Veilleux & Osterbrock 1987; (9) Liu & Kennicutt 1995; (10) Mazzarella & Boroson 1993

medium−low spectral resolutions, allowing fair comparisons with our data. When the flux is available, the observed Hα luminosity (column 8) was estimated. Metallicities (column 9) were determined using the ratio $R_3 = 1.35 \times$ ([O III] λ5007/Hβ) and the empirical relation proposed by Vacca & Conti (1992). For the metallicities of I Zw 18 and II Zw 40, we adopted the values estimated by Izotov, Thuan & Lipovetsky (1998) and Masegosa, Moles & Campos-Aguilar (1994). The activity types (column 10) were established by comparing the ratios [NII] λ6584/Hα and [O III] λ5007/Hβ (Baldwin, Phillips & Terlevich 1981; Veilleux & Osterbrock 1987). The numbers in the last column identify the references for the various spectroscopic data.

We give some information on the FIR for 31 galaxies (64 per cent) in our sample in Table 2. These data come from the *IRAS* Faint Source Catalogue, as found in NED. The FIR luminosity in column 2 was determined using the relation (Londsdale et al. 1985):

$$\log(L_{\rm IR}) = \log(F_{\rm IR}) + 2\log[z(z+1)] + 57.28,$$

where z is the redshift, $F_{\rm IR} = 1.26 \times 10^{-11}(2.58 f_{60} + f_{100})$ erg cm^{-2} s^{-1} and f_{60} and f_{100} are the fluxes in Jansky at 60 and 100 μm respectively. In columns 3 and 4, we also give the FIR spectral indices (Sekiguchi 1987):

$$\alpha(\lambda_1, \lambda_2) = \frac{\log(f_{\lambda_1}/f_{\lambda_2})}{\log(\lambda_2/\lambda_1)}.$$

To facilitate our analysis, only galaxies which have IRAS fluxes

Table 2. FIR characteristics for some galaxies in our sample.

Name	$L_{IR}/L_{\odot}$	$\alpha(60, 25)$	$\alpha(100, 60)$	Act. type
MBG 00027−1645	8.18	−2.11	−1.77	SBNG
MBG 00439−1342	8.61	−2.74	−1.47	SBNG
MBG 00461−1259	10.22	…	−0.73	…
Mrk 1002	10.16	−2.05	−0.61	SBNG
Mrk 363	9.83	…	−0.83	…
MBG 02072−1022	10.70	−1.87	−1.59	SBNG
MBG 02141−1134	10.51	−2.37	−1.33	SBNG
Mrk 1055	10.30	…	−2.32	…
Mrk 602	9.00	−2.03	−0.82	SBNG
KUG 0305−009	9.92	…	−2.22	…
Mrk 603	10.35	−2.04	−0.28	SBNG
MBG 03084−1059	9.83	…	−1.85	…
MBG 03183−1853	9.58	…	−2.66	…
MBG 03468−2217	10.29	−1.98	−0.47	SBNG
IRAS 04493−0553	9.83	−2.53	−1.34	SBNG
Mrk 1194	10.64	−2.57	−1.06	SBNG
Mrk 384	10.45	−2.11	−1.19	SBNG
Mrk 90	9.83	…	−1.60	…
Mrk 102	9.64	…	−1.20	…
Mrk 401	9.42	−1.74	−0.87	SBNG
Mrk 404	9.91	−2.48	−1.35	SBNG
Mrk 710	9.33	−2.16	−0.80	SBNG
MBG 21513−1623	10.72	−2.13	−1.43	SBNG
Mrk 307	10.27	−2.56	−1.70	SBNG
KUG 2300+163	9.11	…	−0.34	…
Mrk 326	10.13	−1.95	−0.79	SBNG
MBG 23318−1156	9.23	…	−1.45	…
Mrk 538	10.31	−1.47	−0.21	SBNG
MBG 23372−1205	9.67	…	−0.96	…
MBG 23388−1514	9.14	…	−1.05	…
Mrk 332	9.91	−2.35	−1.31	SBNG

with high or intermediate qualities had their FIR characteristics estimated. The last column gives the classification of activity type as deduced from FIR criteria (see Section 2.2).

2.3 The nature of the starburst galaxies in our sample and the physical variety of starburst galaxy hosts

In Fig. 1(a) we show the spectroscopic diagnostic diagram used to classify 28 galaxies in our sample using spectroscopic data available in the optical. In this diagram, the horizontal dashed line distinguishes between H II galaxies and SBNGs (Coziol 1996). We count 19 SBNGs for nine H II galaxies. This result confirms our observational bias towards SBNGs. The thin continuous curve in Fig. 1(a) follows the locus traced by normal disc H II regions (Coziol et al. 1994). On this curve, the gas metallicity, given as 12 + log(O/H), increases as the level of excitation (related to [O III]/Hβ) decreases. The galaxies in our sample cover the complete sequence in starburst metallicities. Considering only the SBNGs, we found a mean metallicity of 12 + log(O/H) = 8.7 ± 0.2, which is typical of this class of galaxies (Coziol et al. 1999).

Half of the galaxies that could not be classified in the optical have FIR characteristics which can be used to determine their starburst type: either SBNGs or H II galaxies. In Fig. 1(b) we show a diagnostic diagram based on IRAS spectral indices $\alpha(60, 25)$ and $\alpha(100, 60)$. Starburst galaxies are described in this diagram by a model with two dust components (Sekiguchi 1987): a cold component with a dust temperature of 27 K and a hot component with dust temperatures varying between 70 and 90 K. According to this model, starburst galaxies differ from normal spiral galaxies by their hot dust contribution, which is usually higher than 60 per cent. Although very few H II galaxies are detected in the FIR, they can usually be distinguished from SBNGs from their hotter dust temperatures. This is indicated by the grey area in Fig. 1(b). According to this last criterion, most of the galaxies with FIR data in our sample are SBNGs.

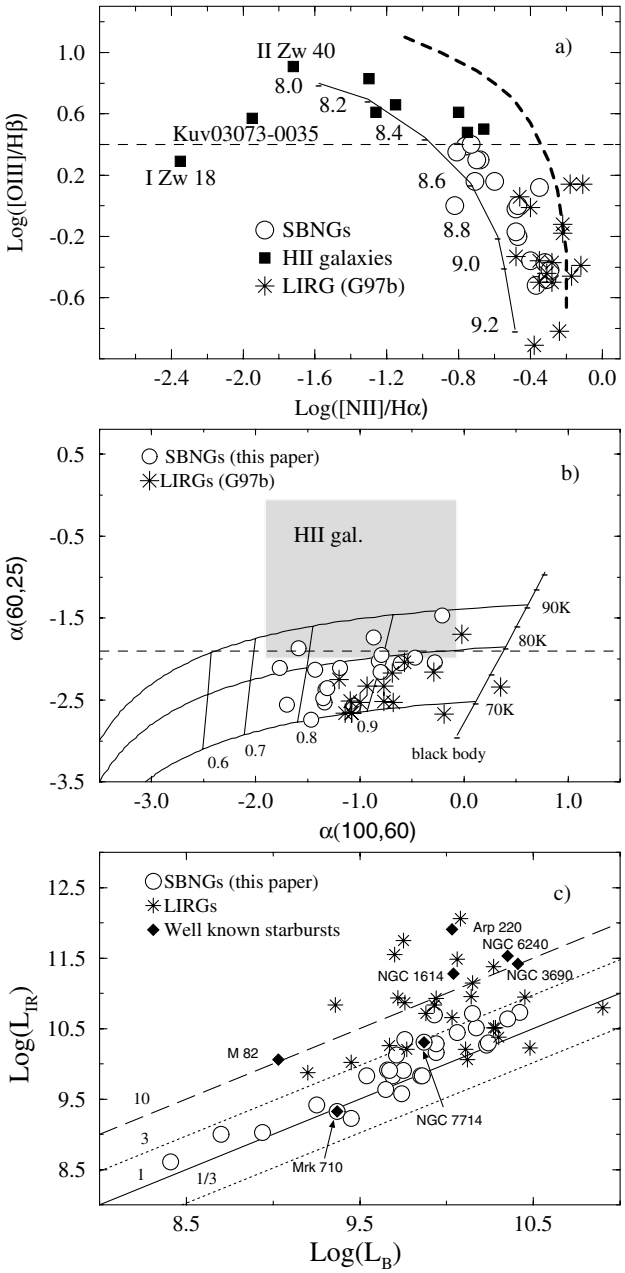

Figure 1. (a) Spectroscopic diagnostic diagram in the optical region. The bold dash curve separates starbursts from AGNs. The horizontal dashed line separates high and low excitation emission-line galaxies. The thin continuous curve is the H II regions sequence in metallicity (solar metallicity =8.84 on this scale). (b) IRAS diagnostic diagram with two blackbody models for dust. The numbers indicate the fractional contribution from hot dust. The horizontal dash line separates SBNGs from AGNs. The grey area is the locus occupied by H II galaxies. (c) FIR versus *B* luminosities. The four diagonal lines correspond to different ratios of L_{IR}/L_B.

2.4 Probability of finding an AGN in our sample

Using FIR criteria, we can also ascertain the probability that one of

the galaxies in our sample is dominated by an AGN. According to Coziol et al. (1998), 99 per cent of IRAS starburst galaxies have $\alpha(60,25) < -1.9$ (the horizontal dashed line in Fig. 1b), while only 25 per cent of Seyfert galaxies have such FIR colours. Almost all the galaxies in our sample have $\alpha(60,25) < -1.9$, which excludes the possibility that one of these galaxies is dominated by an AGN. Note that the three galaxies exceeding this limit in our sample (Mrk 538, Mrk 401 and MBG 02072−1022) have already been classified as SBNGs from their spectra. In fact, all the galaxies previously classified as starburst based on their optical spectra occupy this region of the diagram, which thus confirms their nature as starburst.

Only six of the galaxies detected in the FIR diagram do not have a spectral classification in the optical. Based on the reported statistics above, and the total number of galaxies that was necessary to establish it (see Coziol et al. 1998), we estimate to 7 per cent the probability to find an AGN (which is probably not predominant) in this region of the diagram . This reduces the probability to zero that one of these six galaxies also hosts an AGN. This result is not surprising, considering the moderate FIR luminosity of these galaxies and the fact that the probability of finding an AGN increases with the FIR luminosity (Veilleux, Kim & Sanders 1999).

The above conclusion also holds for the 10 galaxies in our sample without spectral classification or FIR detection. Eight of these galaxies were classified as starburst based on an objective prism spectrum, which rules out the presence of a broad line or luminous AGN. The last two are MBG galaxies and were classified as starburst based on narrow lines and small [NII]/Hα ratios in one spectrum. The fact that these galaxies were not detected in IRAS suggests that the probability of these galaxies hosting an AGN is practically null.

2.5 Comparison with LIRGs and ULIRGs

At this point in our analysis, it is convenient to compare our sample of galaxies with the 16 LIRGs previously classified as starburst in the study of Goldader et al. (1997a). In Fig. 1(a), we see that the LIRGs have spectroscopical characteristics similar to SBNGs. However, they are generally more metal-rich, having solar metallicity on average. Their hot dust contribution (Fig. 1b) is also higher than in SBNGs, which is consistent with their higher FIR luminosity.

In Fig. 1(c), we compare the FIR and B luminosities of our galaxies with those of the LIRGs. For comparison, we also include some ultra luminous infrared galaxies (ULIRGs) from the literature. The ratios of $L_{\rm IR}/L_B$ can be used to distinguish galaxies with unusually high star formation rates (see Coziol 1996): normal late-type spiral galaxies with constant star formation rates over the last 3 Gyr have $1/3 < L_{\rm IR}/L_B < 3$. One can see that the ratio $L_{\rm IR}/L_{\rm B}$ tends to increase with the B luminosity. The ULIRGs and LIRGs both have higher B luminosities and, therefore, higher $L_{\rm IR}/L_B$ ratios as compared to SBNGs. The ratio of $L_{\rm IR}/L_B$ varies between 1 and 3 for most of the galaxies in our sample. This comparison suggests that ULIRGs and LIRGs are generally more massive than SBNGs (having higher B luminosity values) and may have more active burst regions or have younger bursts (as judged from their higher $L_{\rm IR}/L_B$ ratios).

One remarkable feature of Fig. 1(c) is how the starburst galaxies in our sample differ from well-known ULIRGs, like Arp 220 or NGC 6240, 1614 or 3690. The nature of ULIRGs is still in debate. It is not certain that part of the activity observed in these galaxies is not caused by a hidden AGN. This is not the case of the galaxies in our sample. The position, in Fig. 1(c), of the 'prototype' starburst galaxy M82 seems interesting, however. This galaxy looks more like an ULIRG than one of our galaxies. This is consistent with the extreme properties observed in this object, which may also suggest some kind of AGN activity (Seaquist, Frayer & Frail 1997; Allen & Kronberg 1998; Kaaret et al. 2001). Two other archetype starburst galaxies in our sample are NGC 7714 (Mrk 538) and Mrk 710. These two galaxies are more representative of the starburst activity in our sample of galaxies.

The above analysis emphasizes the diversity of physical characteristics of galaxies that host a starburst. Our observations should reveal if this variety of physical characteristics is reflected in their NIR spectral features.

3 OBSERVATIONS

The 2–2.5 μm spectra, studied in this paper, were obtained with the CGS4 spectrometer (Mountain et al. 1990) on UKIRT on the nights of 1992 November 5 and 1993 November 24, 25 and 26. A 75 line mm^{-1} grating was used in first order, providing a resolving power ($\lambda/\delta\lambda$) of ~ 300 in the K band and a spectral coverage encompassing most of the K band. The plate scale was 3 arcsec pixel^{-1} and the slit width was 1 pixel. This aperture was sufficient to cover the central and most luminous part (usually the nucleus) of the galaxies. The slit length was 30 pixels. For all the galaxies, the slit was positioned in the north–south direction on the brightest optical peak as seen from the off-set guider camera. Integration times were generally 10–20 min and sky frames were obtained by nodding 10 pixels along the slit, hence always keeping the object on the slit. Several spectroscopic and photometric standards were also observed during each night. The spectro-photometric accuracy of our spectra is estimated to be ~ 20 per cent. The spectra were reduced under the IRAF environment using IRAF scripts written by one of us (RD). Details on the procedure followed for the reduction can be found in Doyon et al. (1995).

In Table 3, we present the fluxes and equivalent widths of the Brγ and H_2 emission lines as measured in our spectra. These quantities were estimated after rectifying the continuum by fitting a power law ($F_\lambda \propto \lambda^\beta$) from the featureless sections of the spectrum. The choice of a power law is physically justified by the fact that late-stars show approximately Rayleigh–Jeans spectra in the NIR ($F_\lambda \propto \lambda^{-4}$, between 2 and 2.9 μm; see appendix A of Doyon et al. 1994). A χ^2 minimization routine was then used to fit a Gaussian profile to the Brγ emission line. In Table 3, values without an error estimate corresponds to upper limits of 3σ.

In Table 4 we give the exponent (β) of the power-law fit for the continuum, the CO spectroscopic indices ($CO_{\rm spec}$), as defined in Doyon et al. (1994), and the spectroscopic K magnitudes. The $CO_{\rm spec}$ quoted include the uncertainty in the continuum level. In general, the error in $CO_{\rm spec}$ is dominated by this uncertainty, which is less than 0.02 mag. The second column of Table 4 gives the redshifts as deduced from the observed features. These redshifts are in relatively good agreement with the one found in NED. The last column gives the signal-to-noise ratios in our spectra.

For each galaxy in the two tables, we give two sets of data. The first set corresponds to values as measured using an aperture covering 3×9 arcsec^2 (Aperture 1). The second set (the last four columns of each table) corresponds to values measured using an aperture covering only 3×3 arcsec^2 (Aperture 2). In our following analysis, the smaller aperture will be associated to the nucleus of the galaxies.

A few representative spectra are shown in Fig. 2 and Fig. 3. We regroup the spectra in two categories. In the first category, Fig. 2, the galaxies possess strong Brackett γ (Brγ; 2.166 μm) emission.

Table 3. Fluxes and equivalent widths for Brγ and H_2 lines.

Name	z	Aperture 1				Aperture 2			
		$f(\mathrm{Br}\gamma)$ $\times 10^{-15}$ (erg s^{-1})	EW(Brγ) (Å)	$f(\mathrm{H_2})$ $\times 10^{-15}$ (erg s^{-1})	EW(H_2) (Å)	$f(\mathrm{Br}\gamma)$ $\times 10^{-15}$ (erg s^{-1})	EW(Brγ) (Å)	$f(\mathrm{H_2})$ $\times 10^{-15}$ (erg s^{-1})	EW(H_2) (Å)
MBG 00027−1645	0.0269	2.1 ± 0.3	4.1 ± 0.7	1.7 ± 0.3	3.2 ± 0.6	0.7 ± 0.2	2.6 ± 0.8	<0.8	<2.9
MBG 00439−1342	0.0019	<2.7	<3.7	<1.6	<2.1	<0.9	<2.7	<0.7	<2.1
MBG 00461−1259	0.0232	1.8 ± 0.4	11.0 ± 2.7	<0.8	<4.5	0.7 ± 0.2	8.3 ± 1.7	<0.3	<3.2
UM306	0.0175	<0.2	<10.9	<0.2	<7.2	<0.1	<11.2	<0.1	<11.6
Mrk 1002	0.0121	8.8 ± 0.6	8.4 ± 0.6	2.7 ± 0.8	2.5 ± 0.7	5.5 ± 0.4	8.6 ± 0.6	<1.3	<1.9
UM372	0.0395	<0.9	<11.7	<0.7	<8.4	<0.4	<5.4	<0.5	<6.7
Mrk 363	0.0087	<1.0	<3.0	<1.6	<4.4	<0.4	<2.7	<0.6	<3.8
MBG 02072−1022	0.0138	37.4 ± 1.9	10.5 ± 0.5	<11.5	<3.1	25.2 ± 0.8	13.9 ± 0.4	<5.4	<2.8
MBG 02141−1134	0.0149	4.2 ± 0.5	7.7 ± 0.9	2.0 ± 0.4	3.5 ± 0.6	1.7 ± 0.4	7.6 ± 1.7	0.8 ± 0.2	3.5 ± 0.8
Mrk 1055	0.0388	<1.1	<4.2	<1.1	<3.7	<0.8	<4.1	<0.6	<2.8
MRK602	0.0018	<6.1	<7.3	<3.0	<3.5	<5.5	<9.1	<2.2	<3.5
KUG 0305−009	0.0214	1.1 ± 0.3	4.2 ± 1.3	<0.8	<2.8	0.6 ± 0.2	3.9 ± 1.2	<0.6	<3.8
Mrk 603	0.0095	23.5 ± 0.8	22.9 ± 0.8	4.1 ± 0.8	3.7 ± 0.8	16.9 ± 0.4	23.4 ± 0.6	1.4 ± 0.3	1.8 ± 0.4
KUV 03073−0035	0.0236	1.0 ± 0.3	5.0 ± 1.4	<1.0	<4.5	0.6 ± 0.1	5.6 ± 0.9	<0.6	<5.1
MBG 03084−1059	0.0180	<1.2	<4.3	<0.9	<3.3	0.8 ± 0.2	5.4 ± 1.1	<0.5	<3.3
MBG 03183−1853	0.0132	<0.7	<3.0	<1.1	<4.4	<0.4	<3.5	<0.4	<3.8
MBG 03317−2027	0.0047	<1.6	<2.1	<2.8	<3.5	<1.4	<2.8	<1.3	<2.4
KUG 0338+032	0.0228	<0.7	<8.3	<0.8	<8.2	0.4 ± 0.1	5.8 ± 1.8	<0.3	<4.4
MBG 03468−2217	0.0157	8.6 ± 0.7	8.4 ± 0.7	3.3 ± 0.5	3.1 ± 0.4	6.3 ± 0.5	8.2 ± 0.6	1.6 ± 0.4	2.0 ± 0.5
MBG 03523−2034	0.0070	1.3 ± 0.4	5.4 ± 1.7	1.1 ± 0.3	4.7 ± 1.1	<0.5	<3.7	<0.3	<2.0
IRAS04493−0553	0.0095	1.6 ± 0.3	7.4 ± 1.4	0.9 ± 0.3	3.9 ± 1.2	0.5 ± 0.2	6.9 ± 2.3	<0.4	<5.5
Mrk 1089	0.0148	10.7 ± 0.3	84.9 ± 3.9	1.8 ± 0.2	13.5 ± 1.9	3.7 ± 0.2	79.0 ± 4.7	0.9 ± 0.2	18.8 ± 4.5
Mrk 1194	0.0167	5.6 ± 0.5	4.1 ± 0.4	3.7 ± 0.6	2.6 ± 0.4	1.1 ± 0.3	1.8 ± 0.5	1.5 ± 0.3	2.3 ± 0.4
II ZW 40	0.0034	45.1 ± 0.4	264.4 ± 9.3	2.3 ± 0.5	13.0 ± 2.7	34.3 ± 0.4	322.0 ± 15.0	1.2 ± 0.2	11.6 ± 1.4
KUG 0720+335	0.0134	16.9 ± 0.6	18.4 ± 0.7	3.5 ± 0.7	3.6 ± 0.8	13.2 ± 0.4	18.9 ± 0.6	2.1 ± 0.4	2.8 ± 0.5
Mrk 384	0.0155	3.0 ± 1.0	3.7 ± 1.2	<3.1	<3.7	2.0 ± 0.4	5.0 ± 0.9	<1.5	<3.5
KUG 0815+249	0.0075	1.5 ± 0.4	7.7 ± 1.9	<1.0	<4.8	0.6 ± 0.1	5.8 ± 1.1	<0.7	<6.2
KUG 0815+246	0.0091	<0.9	<7.4	<1.4	<10.4	<0.6	<8.5	<0.7	<8.7
KUG 0821+229	0.0253	0.5 ± 0.2	4.2 ± 1.4	<0.9	<7.1	0.5 ± 0.2	8.1 ± 2.5	<0.8	<11.1
KUG 0825+252	0.0071	<0.4	<3.9	<0.7	<6.5	<0.3	<5.5	<0.3	<4.7
Mrk 90	0.0112	<2.0	<4.8	<1.0	<2.4	<0.8	<4.2	<1.0	<4.7
Mrk 102	0.0105	<2.0	<3.5	<2.5	<4.1	1.2 ± 0.4	4.4 ± 1.5	<1.8	<6.2
Mrk 401	0.0061	6.8 ± 0.7	5.2 ± 0.5	<2.4	<1.7	6.4 ± 0.5	7.3 ± 0.6	<1.5	<1.6
IZW 18	0.0020	<2.0	<180.4	<1.3	<85.3	<0.8	<76.5	<0.7	<70.4
Mrk 404	0.0038	11.5 ± 1.3	5.3 ± 0.6	<4.4	<1.9	8.9 ± 0.7	6.1 ± 0.5	3.0 ± 1.0	2.0 ± 0.6
Mrk 710	0.0055	18.3 ± 0.6	36.3 ± 1.2	3.1 ± 0.6	5.7 ± 1.1	15.1 ± 0.4	57.5 ± 2.2	2.3 ± 0.3	8.3 ± 1.2
Mrk 33	0.0040	29.8 ± 0.9	34.0 ± 1.1	3.2 ± 0.8	3.5 ± 0.9	18.6 ± 0.5	33.8 ± 1.0	2.0 ± 0.4	3.5 ± 0.7
MBG 21513−1623	0.0381	0.5 ± 0.1	6.5 ± 1.5	<0.6	<7.0	<0.4	<11.3	<0.3	<7.1
Mrk 307	0.0193	<2.1	<8.9	<1.4	<5.4	1.2 ± 0.3	10.4 ± 2.3	<0.8	<6.3
MBG 22537−1650	0.0138	1.0 ± 0.3	3.5 ± 1.0	<1.2	<4.0	0.6 ± 0.2	4.0 ± 1.0	<0.6	<3.5
KUG 2254+124	0.0256	0.8 ± 0.2	10.6 ± 2.7	<0.8	<9.9	0.4 ± 0.1	8.8 ± 2.8	<0.5	<10.8
KUG 2300+163	0.0082	1.3 ± 0.2	21.4 ± 2.5	<0.5	<7.0	0.6 ± 0.1	22.0 ± 2.8	<0.2	<5.9
Mrk 326	0.0140	5.2 ± 0.6	5.3 ± 0.6	<2.4	<2.3	6.1 ± 0.4	8.4 ± 0.6	2.4 ± 0.6	3.1 ± 0.8
MBG 23318−1156	0.0206	0.9 ± 0.2	12.9 ± 3.0	<1.0	<12.4	0.5 ± 0.2	15.4 ± 4.9	<0.4	<10.1
Mrk 538	0.0110	14.6 ± 0.9	17.1 ± 1.1	6.7 ± 1.0	7.5 ± 1.1	10.5 ± 0.4	18.9 ± 0.7	3.2 ± 0.3	5.4 ± 0.6
MBG 23372−1205	0.0239	0.8 ± 0.2	9.0 ± 2.7	<0.7	<7.6	<0.9	<21.3	<0.8	<16.8
MBG 23388−1514	0.0303	<1.6	<23.3	<1.6	<23.0	<0.5	<13.7	<0.6	<14.8
Mrk 332	0.0110	2.5 ± 0.8	2.6 ± 0.8	2.6 ± 0.7	2.6 ± 0.7	2.2 ± 0.6	3.7 ± 0.9	1.9 ± 0.5	2.9 ± 0.8

These galaxies also show relatively strong He I (2.059 μm) and H_2 1-0 S(1) (2.122 μm) emission lines. They show, on the other hand, different strengths of the CO absorption band longward of 2.293 μm.

The most extreme case in our sample is the H II galaxy II Zw 40. This galaxy shows very strong emission lines and an extremely weak CO band. This galaxy also happens to be one of the less chemically evolved galaxies in our sample. Two SBNGs with intense emission lines are Mrk 710 and Mrk 1089. Most galaxies in our sample resemble Kug 0720+335 and Mrk 538 (NGC 7714), which have medium intensity emission lines and a relatively strong CO band.

In the second category, Fig. 3, we find galaxies which have weaker emission lines than Mrk 538 and a somewhat stronger CO band. In some galaxies, like Mrk 332, the NIR emission lines are barely visible, and only upper limits can be measured.

The NIR spectra of our sample of galaxies show significant variations. This result indicates that the diversity of physical characteristics of starburst galaxy hosts, as observed in the optical and far-infrared, implies some variety of the NIR spectral features. Synthetic starburst models will now be used in order to understand what these variations mean in terms of the burst characteristics.

4 NIR ANALYSIS

4.1 Synthetic starburst models: duration, age of burst and IMF

Using synthetic starburst models, it is possible to interpret NIR features like equivalent width of BRγ, EW(Brγ), and CO_{spec} in

Table 4. Continuum slope, CO index and K magnitudes.

Name	z	Aperture 1 β	Aperture 1 CO_{spec} (mag.)	Aperture 1 M_K	Aperture 1 S/N	Aperture 2 β	Aperture 2 CO_{spec} (mag.)	Aperture 2 M_K	Aperture 2 S/N
MBG 00027−1645	0.0269	−2.85 ± 0.14	0.21 ± 0.01	12.32	116	−3.01 ± 0.14	0.25 ± 0.01	13.04	92
MBG 00439−1342	0.0019	−3.15 ± 0.13	0.23 ± 0.01	12.14	115	−2.90 ± 0.10	0.20 ± 0.01	12.99	92
MBG 00461−1259	0.0232	−3.33 ± 0.23	0.17 ± 0.02	13.55	49	−3.27 ± 0.23	0.17 ± 0.02	14.23	48
UM306	0.0175	−4.37 ± 0.35	−0.02 ± 0.04	15.74	26	−3.66 ± 0.44	0.03 ± 0.05	16.49	23
Mrk 1002	0.0121	−2.40 ± 0.10	0.19 ± 0.01	11.59	101	−2.03 ± 0.08	0.17 ± 0.01	12.09	111
UM372	0.0395	−3.11 ± 0.34	0.02 ± 0.03	14.22	23	−3.84 ± 0.25	0.03 ± 0.03	14.32	50
Mrk 363	0.0087	−3.08 ± 0.10	0.15 ± 0.01	12.85	108	−3.01 ± 0.12	0.14 ± 0.01	13.72	92
MBG 02072−1022	0.0138	−2.80 ± 0.13	0.29 ± 0.01	10.34	53	−3.06 ± 0.12	0.32 ± 0.01	11.09	272
MBG 02141−1134	0.0149	−3.01 ± 0.12	0.20 ± 0.01	12.34	85	−2.56 ± 0.13	0.15 ± 0.01	13.26	54
Mrk 1055	0.0388	−3.61 ± 0.21	0.16 ± 0.02	12.95	49	−4.01 ± 0.21	0.21 ± 0.02	13.33	60
Mrk 602	0.0018	−2.97 ± 0.17	0.22 ± 0.01	11.93	132	−2.93 ± 0.19	0.20 ± 0.02	12.27	185
KUG 0305−009	0.0214	−2.90 ± 0.12	0.17 ± 0.01	13.12	70	−2.31 ± 0.13	0.15 ± 0.01	13.70	73
Mrk 603	0.0095	−2.83 ± 0.08	0.16 ± 0.01	11.61	107	−2.79 ± 0.07	0.17 ± 0.01	11.99	187
KUV 03073−0035	0.0236	−2.49 ± 0.14	0.23 ± 0.02	13.28	73	−2.50 ± 0.14	0.26 ± 0.02	13.94	68
MBG 03084−1059	0.0180	−2.74 ± 0.14	0.20 ± 0.01	13.02	63	−2.95 ± 0.15	0.25 ± 0.01	13.73	52
MBG 03183−1853	0.0132	−3.24 ± 0.12	0.16 ± 0.01	13.19	67	−3.35 ± 0.16	0.15 ± 0.01	14.17	55
MBG 03317−2027	0.0047	−3.03 ± 0.10	0.22 ± 0.01	12.01	80	−2.90 ± 0.10	0.21 ± 0.01	12.43	90
KUG 0338+032	0.0228	−3.11 ± 0.23	0.12 ± 0.02	14.24	30	−3.40 ± 0.21	0.12 ± 0.03	14.53	46
MBG 03468−2217	0.0157	−2.36 ± 0.10	0.27 ± 0.01	11.61	85	−2.51 ± 0.10	0.28 ± 0.01	11.93	129
MBG 03523−2034	0.0070	−2.60 ± 0.18	0.21 ± 0.02	13.22	42	−2.40 ± 0.15	0.23 ± 0.02	13.90	49
IRAS 04493−0553	0.0095	−3.04 ± 0.15	0.18 ± 0.02	13.35	37	−2.49 ± 0.23	0.16 ± 0.03	14.50	21
Mrk 1089	0.0148	−2.45 ± 0.32	0.19 ± 0.04	13.83	26	−3.68 ± 0.45	0.16 ± 0.05	14.97	18
Mrk 1194	0.0167	−2.66 ± 0.09	0.22 ± 0.01	11.33	240	−2.67 ± 0.09	0.21 ± 0.01	12.22	222
II ZW 40	0.0034	−1.97 ± 0.15	0.07 ± 0.01	13.42	64	−1.79 ± 0.18	0.06 ± 0.02	13.91	73
KUG 0720+335	0.0134	−2.66 ± 0.08	0.24 ± 0.01	11.72	120	−2.75 ± 0.08	0.26 ± 0.01	12.02	169
Mrk 384	0.0155	−3.11 ± 0.12	0.25 ± 0.01	11.91	52	−2.13 ± 0.12	0.16 ± 0.01	12.60	42
KUG 0815+249	0.0075	−3.19 ± 0.21	0.16 ± 0.02	13.40	51	−3.90 ± 0.20	0.16 ± 0.02	14.09	49
KUG 0815+246	0.0091	−3.20 ± 0.24	0.14 ± 0.02	13.91	35	−3.45 ± 0.31	0.12 ± 0.04	14.55	35
KUG 0821+229	0.0253	−3.28 ± 0.30	0.11 ± 0.03	13.87	34	−4.25 ± 0.27	0.14 ± 0.02	14.57	33
KUG 0825+252	0.0071	−3.06 ± 0.17	0.18 ± 0.01	14.19	36	−3.56 ± 0.21	0.15 ± 0.01	14.89	36
Mrk 90	0.0112	−3.24 ± 0.18	0.22 ± 0.02	12.66	58	−2.98 ± 0.13	0.16 ± 0.01	13.41	50
Mrk 102	0.0105	−3.68 ± 0.14	0.18 ± 0.01	12.29	71	−3.16 ± 0.16	0.12 ± 0.01	13.06	55
Mrk 401	0.0061	−2.91 ± 0.08	0.21 ± 0.01	11.43	286	−2.80 ± 0.08	0.22 ± 0.01	11.86	306
I ZW 18	0.0020	−3.63 ± 3.36	0.43 ± 0.34	16.45	2	−6.69 ± 2.88	−0.01 ± 0.29	16.89	3
Mrk 404	0.0038	−2.69 ± 0.11	0.24 ± 0.01	10.85	91	−2.38 ± 0.08	0.23 ± 0.01	11.26	88
Mrk 710	0.0055	−2.06 ± 0.22	0.09 ± 0.02	12.33	64	−1.65 ± 0.24	0.10 ± 0.03	13.02	71
Mrk 33	0.0040	−2.63 ± 0.10	0.20 ± 0.01	11.80	95	−2.57 ± 0.08	0.19 ± 0.01	12.31	117
MBG 21513−1623	0.0381	−2.60 ± 0.26	0.14 ± 0.02	14.26	32	−3.18 ± 0.45	0.12 ± 0.05	15.22	23
Mrk 307	0.0193	−3.24 ± 0.23	0.21 ± 0.02	13.19	49	−2.98 ± 0.22	0.24 ± 0.02	13.96	38
MBG 22537−1650	0.0138	−2.70 ± 0.11	0.16 ± 0.01	12.92	78	−2.88 ± 0.13	0.17 ± 0.01	13.60	92
KUG 2254+124	0.0256	−3.84 ± 0.25	0.10 ± 0.03	14.33	25	−4.65 ± 0.31	0.20 ± 0.04	14.98	31
KUG 2300+163	0.0082	−2.54 ± 0.22	0.19 ± 0.02	14.61	44	−2.49 ± 0.21	0.17 ± 0.02	15.58	52
Mrk 326	0.0140	−2.87 ± 0.10	0.24 ± 0.01	11.67	105	−2.68 ± 0.10	0.27 ± 0.01	12.00	166
MBG 23318−1156	0.0206	−3.67 ± 0.34	0.05 ± 0.03	14.44	24	−3.59 ± 0.34	0.11 ± 0.04	15.29	19
Mrk 538	0.0110	−3.11 ± 0.13	0.22 ± 0.01	11.83	82	−3.19 ± 0.13	0.27 ± 0.01	12.31	79
MBG 23372−1205	0.0239	−3.28 ± 0.49	0.09 ± 0.05	14.22	22	−3.16 ± 0.75	0.07 ± 0.08	15.04	18
MBG 23388−1514	0.0303	−5.80 ± 0.78	−0.12 ± 0.08	14.59	13	−5.33 ± 0.57	−0.03 ± 0.07	15.30	13
Mrk 332	0.0110	−3.51 ± 0.15	0.21 ± 0.01	11.75	129	−3.45 ± 0.15	0.23 ± 0.01	12.22	153

terms of the duration of the burst, its age and the form of the IMF (Puxley, Doyon & Ward 1997; Leitherer & Heckman 1995; Mayya 1997). The principal steps in the synthetic starburst model are the following (Leitherer & Heckman 1995).

(i) Stars are formed at specified rates and distributed along the HR diagram.

(ii) Evolutionary models describe the time-dependence of the individual physical parameters of the stars (mass, luminosity, etc.

(iii) The stellar number densities in the HR diagrams are determined and any desired synthetic quantities assigned to each stars.

By summing over the entire stellar population, the model yields the *integrated properties* of starburst galaxy.

In these models, star formation is represented by an exponential law: $\xi(t) = \xi(t = 0) \exp\ -t/\tau$, where t is the age of the burst and τ its duration. Two limiting cases are of special interest: an instantaneous burst and a constant star formation rate. An instantaneous burst corresponds to the case where the duration of star formation is short compared to the age of the galaxy ($\tau \ll t$). All the stars are thus formed at the same epoch. The other limiting case is a constant star formation rate (CSFR). This mode of star formation is characteristic today of discs in giant spiral galaxies (Kennicutt 1983).

It is important to note that theoretically a CSFR can always be approximated as a series of instantaneous bursts. It means that a system having experienced a sequence of bursts over a time period comparable to $\tau = t$ would be observationally indistinguishable from a galaxy with a CSFR (Leitherer et al. 1999).

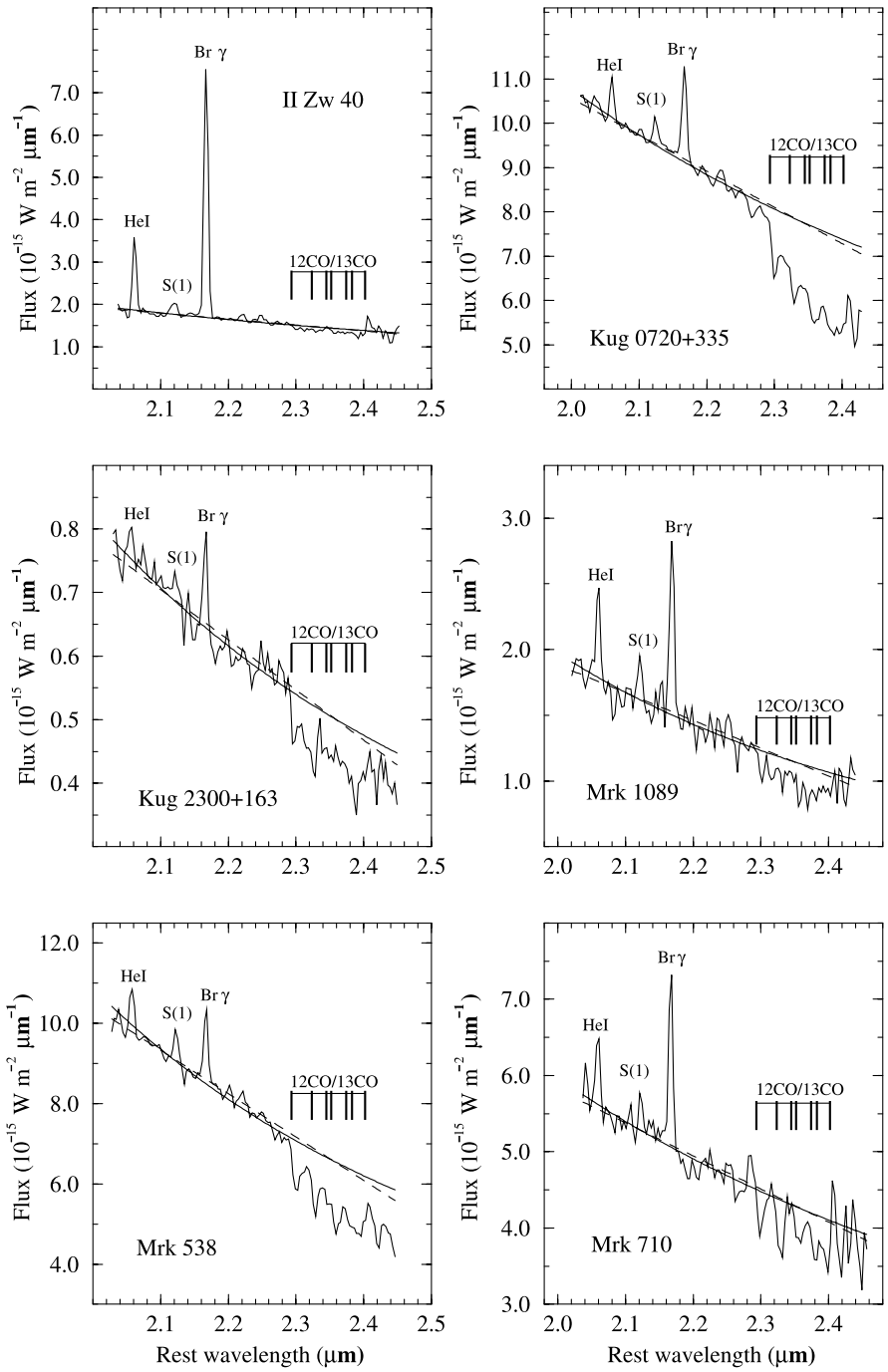

Figure 2. Some examples of spectra with strong Bracket γ emission line. The spectra were shifted to their rest frame using velocities in Table 1. Conspicuous emission lines and absorption features are identified. For each galaxy we show the power law fitted on the continuum and the window used to measure CO_{spec}. We also show a straight-line fit. A straight line does not give a good fit for the *K* continuum of late-type stars and galaxies. However, it would have no significant effects on the measurements of the CO_{spec} (variation < 1 per cent).

Another important parameter in the synthetic starburst model is the IMF. This function is usually expressed as a power law: $\phi(M) = Cm^{-\alpha}$, where the constant C is determined by the total mass converted into stars. To get the whole spectrum of star masses formed, the IMF is integrated between the upper and lower mass cut-offs, M_{up} and M_{low}. In starburst models, the exponent of the IMF and the two mass cut-offs are not very well constrained and it is therefore important to try different possible values.

We choose to compare our data with the models of Leitherer et al. (1999). These authors have made their grids of results directly accessible on the World Wide Web.[1] We consider only two limiting cases: the instantaneous burst and the CSFR ($1\,M_\odot\,yr^{-1}$). For each of these cases, three different scenarios are tested: (i) a Salpeter IMF, $\alpha = 2.5$, with $M_{up} = 100\,M_\odot$; (ii) a Salpeter IMF with $M_{up} = 30\,M_\odot$; (iii) an IMF with a steeper slope, $\alpha = 3.3$ and $M_{up} = 100\,M_\odot$. The models cover ages from 10^6 to 10^9 yr.

[1] http://www.stsci.edu/science/starburst

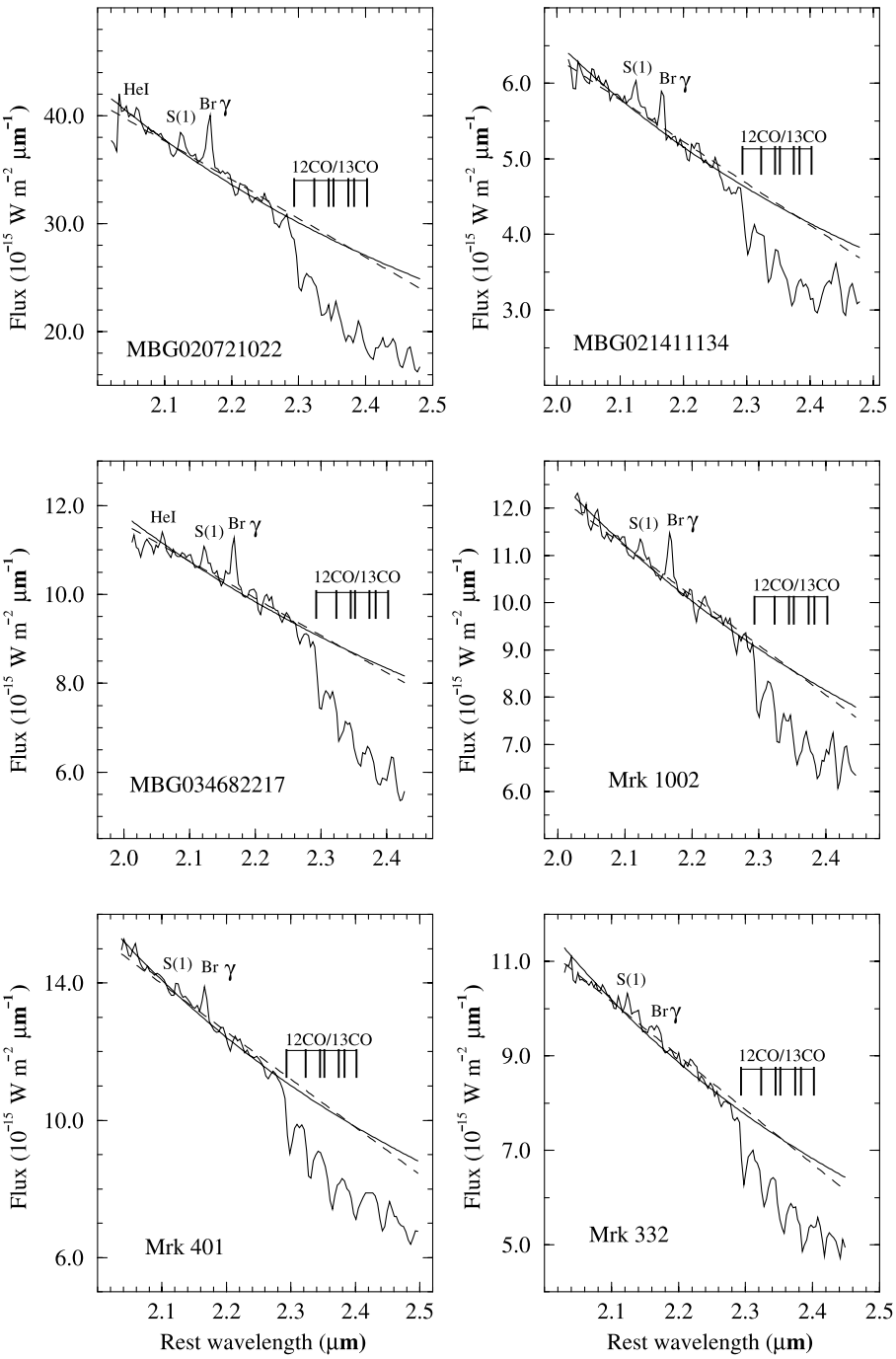

Figure 3. Examples of spectra with a relatively weak Bracket γ emission line and strong CO lines. The spectra are as described in Fig. 2.

Comparisons of our data for EW(Brγ) and CO_{spec} with the instantaneous burst models are presented in Fig. 4. From this figure, we conclude that none of the instantaneous burst models can fit the ensemble of our data. For solar metallicity ($Z = 0.02$), the models generally underestimate the value of EW(Brγ). Some galaxies can be fitted by instantaneous bursts, but the predicted metallicity is $2\,Z_{\odot}$, which is much higher than the gas metallicity we have estimated in these galaxies. Our results confirm those of Goldader et al. (1997b), extending their conclusion to starburst galaxies with different physical properties and FIR luminosity. It implies that the instantaneous burst scenario is not a good representation of the starburst phenomenon.

Our data are compared with the CSFR models in Fig. 5. One can see in Fig. 5(a) that the Salpeter IMF model with $M_{up} = 100\,M_{\odot}$ cannot fit the ensemble of our data. However, a relatively good fit is obtained in Fig. 5(b) when the upper mass cut-off is equal to $M_{up} = 30\,M_{\odot}$. We see no improvement in Fig. 5(c) after adopting an IMF slope of $\alpha = 3.3$.

Once again, our results confirm those of Goldader et al. (1997b), extending their conclusion to all the starburst types known. We conclude that the best parameters which describe starburst galaxies in the nearby Universe are a CSFR and a Salpeter IMF with an upper mass cut-off $M_{up} = 30\,M_{\odot}$.

According to this solution, the bursts have ages between 10 Myr

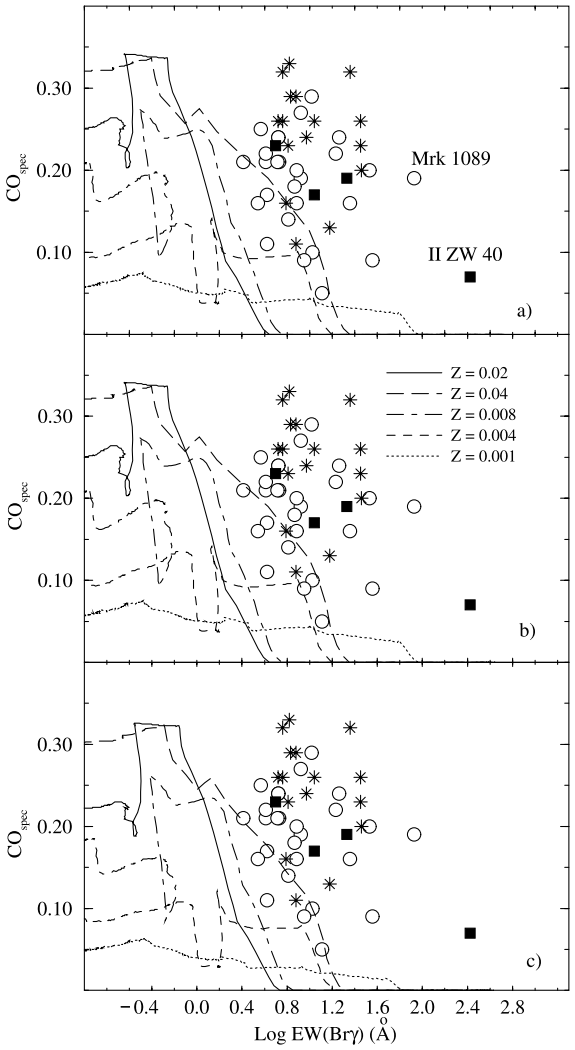

Figure 4. Comparison of our data with instantaneous burst models. (a) An IMF with a slope of $\alpha = 2.5$ and an upper mass limit of $M_{up} = 100\,M_\odot$. (b) An IMF with a slope of $\alpha = 2.5$ and an upper mass limit of $M_{up} = 30\,M_\odot$. (c) An IMF with a slope of $\alpha = 3.3$ and an upper mass limit of $M_{up} = 100\,M_\odot$. The models cover ages from 10^6 to 10^9 yr. (Open circle = SBNG, filled square = H II galaxy, star = LIRG.)

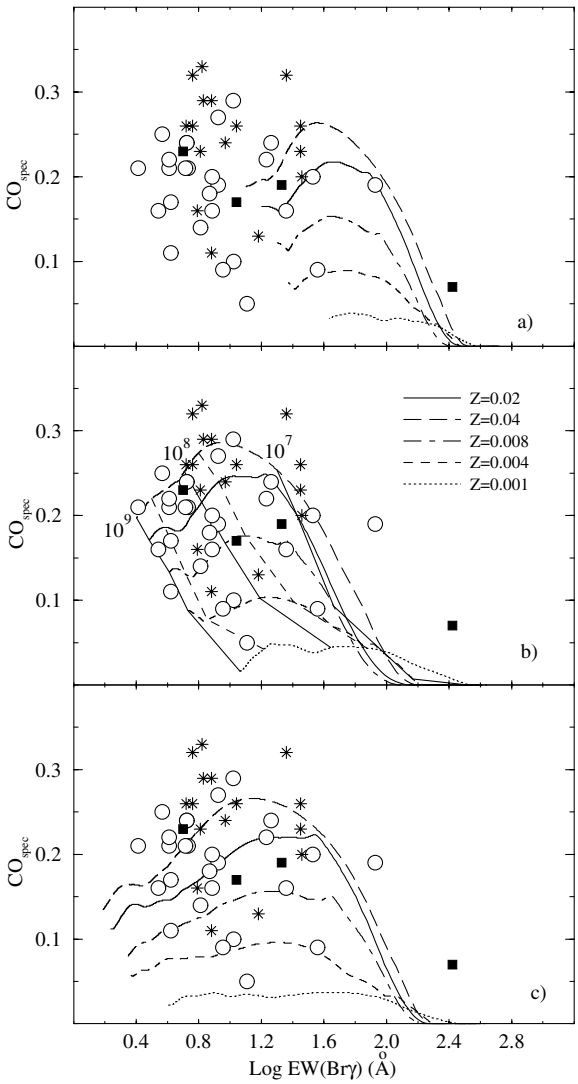

Figure 5. Comparison of our data with constant star formation models ($1\,M_\odot$ per yr). (a) An IMF with a slope of $\alpha = 2.5$ and an upper mass limit of $M_{up} = 100\,M_\odot$. (b) An IMF with a slope of $\alpha = 2.5$ and an upper mass limit of $M_{up} = 30\,M_\odot$. (c) An IMF with a slope of $\alpha = 3.3$ and an upper mass limit of $M_{up} = 100\,M_\odot$. The significance of the symbols is the same as in Fig. 4.

and 1 Gyr, the majority being older than 100 Myr. Comparing with LIRGs, we found, on average, younger bursts for these galaxies, with ages lower than 100 Myr. This is consistent with the difference in luminosity ratios noted in Section 2.5. The model also correctly reproduces the fact that LIRG are more metal-rich than the SBNGs. The consistency with the metallicities deduced from their optical spectra (Section 2.2) is remarkably good.

According to the model, H II galaxies must have younger bursts than the SBNGs. The metallicities predicted by the models are also in good agreement with those measured. Young bursts and low metallicities are also consistent with the higher dust temperatures suggested by the FIR model in Section 2.3.

In our sample, the galaxy which have the youngest burst is II Zw 40. The position of this galaxy in Fig. 5(a) suggests that it may be possible to fit an IMF with an upper mass cut-off of $M_{up} = 100\,M_\odot$ (although the predicted metallicity would then be wrong). The same conclusion may also apply to Mrk 1089. These observations may suggest varying IMF in some galaxies (Doyon et al. 1992).

From the above discussion, we conclude that the solution of the synthetic starburst model is consistent with observations in the optical and FIR regions. In particular, it satisfactorily explains the differences between the different starburst types: H II galaxies have younger bursts and lower metallicities than SBNGs, while LIRGs have younger bursts but higher metallicities. These differences may be related to different histories of star formation or different stages in burst evolution.

Taken at face value, the above result confirms the studies of Doyon et al. (1992), Goldader et al. (1997b) and Coziol (1996). The generality of our observation further suggests that this must be a characteristic of starburst galaxies in the nearby Universe. However, the above solution may not represent strong constraints on the duration of the burst or the IMF. This is because the synthetic starburst models we used cannot distinguish between real constant star formation and a series of instantaneous bursts (Leitherer et. al 1999). In order to verify this alternative, we will now re-examine our spectra and search for traces of previous bursts.

4.2 Spatial variation of NIR features: evidence for sequences of bursts

In order to reproduce CSFR using a sequence of bursts, one must assume that this sequence spreads over a relatively long period of time. The solution of the synthetic starburst model suggests a period extending over the range from 10^8 up to 1 Gyr. If this sequence of burst is related to some self-regulated mechanism or to the propagation of star formation, we may also assume that the different bursts do not happen in the same regions of space. This implies that the bursts regions should be heterogeneous in space and time. With sufficient spatial resolution, we should then observe a variation in burst characteristics as we survey different regions. As a first test, therefore, we can check if a variation of aperture in our spectra induces some variation of the NIR spectral features.

Before doing the aperture test, it is important to verify that the obvious increase of scale with distance, implied by our two fixed apertures, does not introduce any systematic variations, which could be misinterpreted as variation of burst characteristics. Associating the smaller aperture (3×3 arcsec^2) to the nucleus, we verify in Fig. 6 that the ratios of the Brγ fluxes and equivalent widths, as measured in and out of the nucleus, do not show any relation with the redshift. Similar negative results were also obtained for H_2, the K magnitudes, the CO_{spec} and the slope of the continuum (β). These negative results suggest that whatever variations we may observe for these ratios, their origin must be intrinsic to each galaxy.

Having verified that the two fixed apertures do not introduce spurious effects, we now proceed to examine how the different ratios varied in each galaxy. In Fig. 7(a), we first compare the ratios of the fluxes in Brγ with the ratios of the equivalent widths. In general, the ratios $f(\mathrm{Br}\gamma)/f(\mathrm{Br}\gamma)_N$ are greater than one, which indicates that the bursts of star formation generally extend over a few kpc around the nucleus. The equivalent widths, on the other hand, are generally wider in the nucleus, except in galaxies where the ratio $f(\mathrm{Br}\gamma)/f(\mathrm{Br}\gamma)_N > 2$, which corresponds to extended bursts, and where the equivalent width stays constant or increases out of the nucleus. According to synthetic starburst models, EW(Brγ) is an indicator of the age of the burst. From the above observation we then deduce that in the galaxies where the star formation is more concentrated, the bursts are younger in the nucleus. The contrary seems to be true in galaxies where the bursts are more extended. No difference is observed between H II galaxies and SBNGs.

The case for H_2, Fig. 7(b), is slightly different. Very few galaxies in our sample show significant H_2 emission. In these galaxies we find the same tendency as for Brγ, which is that the H_2 emission generally spreads out of the nucleus. However, the H_2 equivalent width tends to be wider out of the nucleus. In Fig. 7(c) one can see that in galaxies where the star formation is concentrated in the nucleus [$f(\mathrm{Br}\gamma)/f(\mathrm{Br}\gamma)_N < 2$], the H_2 emission is more intense than Brγ emission out of the nucleus. Only two galaxies, Mrk 1089 and Mrk 1194, show the reverse tendency. For the galaxies in our sample with a significant amount of H_2 emission, the H_2 emission seems, therefore, to be always more intense and widespread in regions where Brγ is less intense and less abundant. We also verified that 50 per cent of the galaxies without H_2 detection have detectable Brγ emission, which is consistent with the observed general tendency. The signification of this variation is not obvious, however, and its possible interpretation will therefore be kept for later on during our analysis.

For the K-band magnitude, we naturally expect it to increase as

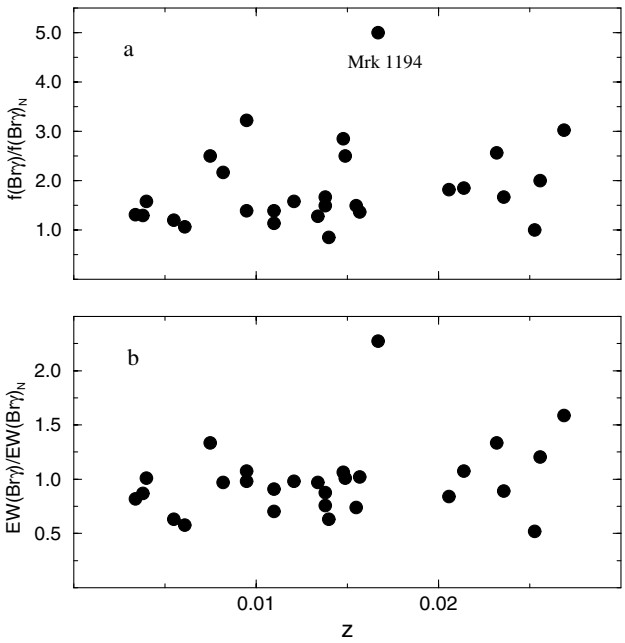

Figure 6. Comparison of (a) the ratios of Brγ fluxes and (b) of of the equivalent widths, as measured in and out of the nucleus and as functions of the redshift. In this analysis we associate the smaller aperture (3×3 arcsec^2) to the nucleus. No relation with redshift is observed, which indicates that the increase of scale with distance, implied by our two fixed apertures, does not introduce any systematic variations. The galaxy showing the higher variation is Mrk 1194. No particular reasons explain this variation.

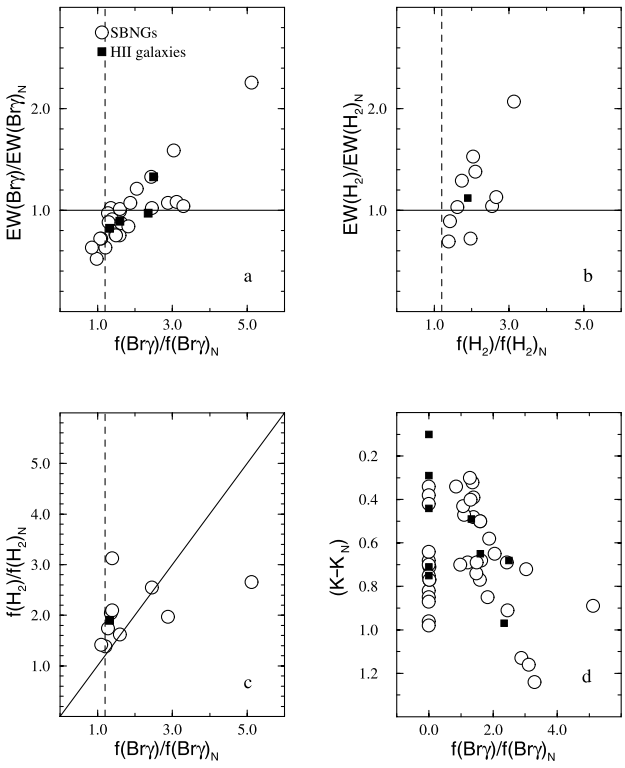

Figure 7. Variation of the NIR features as measured in two different apertures. We compare the values measured in a 3×3 arcsec^2 aperture (nucleus) with those in a larger 3×9 arcsec^2 aperture. The vertical dashed line in panels (a), (b) and (c) is the limit adopted for spatial resolution.

the number of stars included in the aperture increases. However, the mean variation observed in Fig. 7(d) seems smaller than what we expected. While the gain in surface represented by the difference in aperture is a factor of 3, we find a meager $\Delta K = -0.7$, which corresponds to an increase in flux by only a factor of 1.8. The *K*-band emission, therefore, seems mostly concentrated in the nucleus. Indeed, one can see in Fig. 7(d) that the difference in *K*-band magnitude is smaller in galaxies where the bursts are concentrated $[f(\mathrm{Br}\gamma)/f(\mathrm{Br}\gamma)_N < 2]$ than in galaxies where the bursts are extended. The *K*-band emission seems, therefore, to closely follow the region of the bursts. This observation suggests that the stars emitting in the *K* band must be very closely related to the bursts.

No trend was observed for $\mathrm{CO}_{\mathrm{spec}}$ or β. These two parameters show random variations with standard deviations of ± 0.04 for the difference in $\mathrm{CO}_{\mathrm{spec}}$ and ± 0.15 for the ratios of β.

To illustrate what effects the variations of NIR features have on the burst characteristics of each galaxy, we show in Fig. 8 the changes introduced by an increase in aperture in the burst model of Fig. 5(b). In this figure, an increase in the equivalent width results in a younger age while an increase in the $\mathrm{CO}_{\mathrm{spec}}$ results in an increase of metallicity and a younger age. In Fig. 8, one can see that some variations may imply significant differences in terms of the burst characteristics. No trend is observed, however, which suggests that the cause of these variations may depend on the particular history of star formation of each galaxy. Higher spatial resolution will be necessary to confirm this result.

From the above analysis we conclude that the variation of the NIR spectral features with aperture are consistent with a variation of burst characteristics in space. This result supports our hypothesis that the burst regions are not homogeneous in space. However, the absence of systematic trends and the lack of spatial resolution impede us in discovering the real cause of this variation and we must therefore search for other evidence in favour of the multiple burst hypothesis.

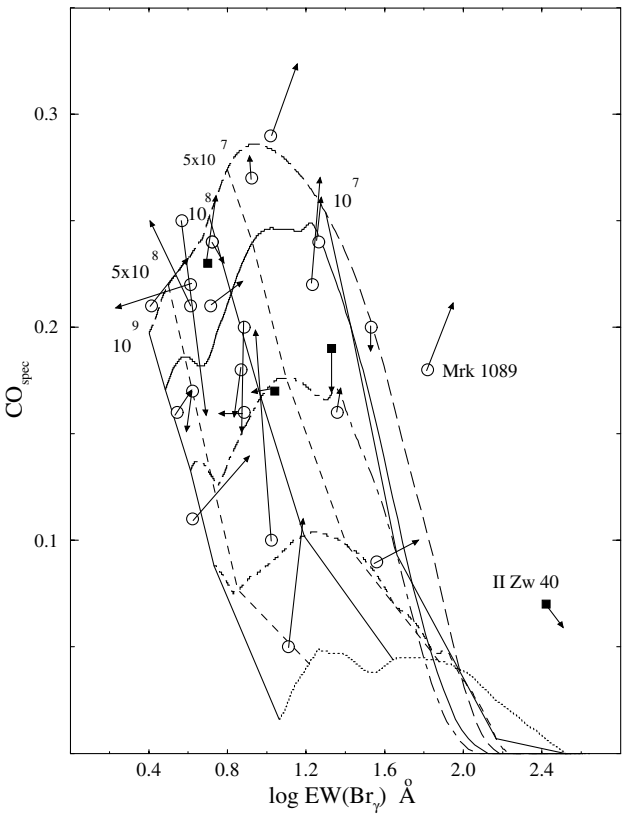

Figure 8. Variation of the burst characteristics with a variation in aperture. The parameters of the model are the same as in Fig. 5(b).

4.3 Luminosity–luminosity relations

Our previous analysis suggests that the stars emitting in the *K* band are tightly related to the burst population. We should then expect to find a good correlation between the *K*-band absolute magnitude and parameters linked to the burst. This is important to verify, because the stars producing the *K*-band luminosity are probably the same stars which produce the CO band. A correlation of *K*-band luminosity with parameters directly linked to the burst would thus favour massive and young stars, namely RSGs, over older stars like RGs.

We see in Fig. 9(a) that the luminosity $L(\mathrm{Br}\gamma)$ increases with the *K*-band absolute magnitude. A linear regression performed on our data (continuous curve in Fig. 9a) gives a weak but statistically significant coefficient of correlation, $R = 67$ per cent (with 33 points, the probability in obtaining a higher correlation by chance is $P_{33,0.67} < 0.05$ per cent; Pugh & Winslow 1966). The correlation improves to 82 per cent when we include the LIRGs (dashed curve in Fig. 9a). The properties of our galaxies are in good continuity with those of the LIRGs, which form the upper limit of the distribution.

The correlation of $L(\mathrm{Br}\gamma)$ with the *K*-band absolute magnitude confirms that the stars producing this luminosity are related to the burst population. The relative weakness of this relation, however, may suggest that they are not correlated to the younger stars. However, this result is consistent with what we expect if the stars emitting in the *K* band are mostly RSGs: the number of RSGs increases with the intensity of the burst, but these stars also only appear in great number after the peak intensity of the bursts.

In Fig. 9(b), we find a reverse tendency for $\mathrm{EW}(\mathrm{Br}\gamma)$, as this parameter decreases as M_K increases. These two parameters are not strongly correlated ($R = 57$ per cent), although the correlation is still statistically significant ($P_{33,0.57} < 0.05$ per cent). The obvious interpretation for this reverse tendency is that galaxies that are richer in burst regions naturally also contain the highest number of evolved stars.

What is interesting in this last figure is the high dispersion of the data. This high dispersion suggests that the evolution of the bursts depends on the particular star formation history of each galaxy. This is consistent with our analysis of the variation with aperture and also suggests that the bursts may be heterogeneous in time [the dispersion in $\mathrm{EW}(\mathrm{Br}\gamma)$ is a dispersion in time]. The behaviour of the LIRGs is particularly remarkable, suggesting younger bursts than the observed tendency would have predicted. This could be one indication of repetitive bursts.

Note that we do not reject, a priori, the alternative, which is that the stars emitting in the *K* band are old RGs. In this case, the correlation of M_K with $L(\mathrm{Br}\gamma)$ would suggest some relation between the mass and intensity of the bursts, while the correlation between M_K and $\mathrm{EW}(\mathrm{Br}\gamma)$ would mean that the bursts evolve more rapidly in galaxies where they are more intense. However, it would be difficult in this case to understand why the correlations are not stronger. However, such interpretations are in fact much more constraining than what our data can reveal (we do not have information on the masses or the intensity of the bursts, which should be normalized by the surface or volume anyway). To our knowledge, such relations were never reported before, and our data

are obviously insufficient to defend them. Our favoured interpretation, on the other hand, does not imply any new mechanisms, relying only on standard star evolutionary scenarios. Another argument in favour of our interpretation may be the relatively strong correlation we find between $L(H_2)$ and M_K, as we now show.

A very strong correlation, $R = 92$ per cent, is found between $L(H_2)$ and M_K in Fig. 10(a). The lower number of points in this fit does not influence the results: with 16 points, the probability of obtaining a higher correlation by chance is $P_{16,0.92} < 0.05$ per cent. This good correlation does not depend on the inclusion of the LIRGs either, the coefficient only increasing to $R = 94$ per cent when we include them. For the equivalent widths, shown in Fig. 10(b), we also find a better correlation than for Brγ, $R = 62$ per cent and $P_{16,0.62} < 1.4$ per cent. This behaviour suggests that the H_2 emission is better correlated to a more evolved phase of the bursts, being correlated to SRGs, than to a younger phase. In general, therefore, the behaviour of H_2 emission seems consistent with the hypothesis of heterogeneous bursts in space and time, showing variations with aperture (Section 4.2) and the coexistence of evolved and younger components. It would help, however, to determine what the process that produces this line is, as the two most probable mechanisms, supernovae shock remnants and UV fluorescence, imply much different time-scales.

In principle, it would be possible to determine what the mechanism is that produces the H_2 emission by comparing the two luminosities $L(\mathrm{Br}\gamma)$ and $L(H_2)$. In Fig. 11 we find that $L(H_2)$ is relatively well-correlated to $L(\mathrm{Br}\gamma)$ ($R = 74$ per cent with $P_{16,0.62} < 0.4$ per cent). However, the ratios of $L(\mathrm{Br}\gamma)/L(H_2)$ stay between 0.1 and 1, which is consistent with supernovae shock remnants (Moorwood & Oliva 1990) or UV fluorescence (Puxley, Hawarden & Mountain 1990). Therefore, although our observations suggest that the H_2 emission phenomenon is related to a more evolved phase of the bursts, we are unable to say if this phase happens a few 10^6 (the time-scale of supernovae), 10^7 or 10^8 yr (the time-scale of B stars, responsible for UV fluorescence) after the maximum of the bursts.

4.4 Spectral types of ionizing stars

In Coziol & Demers (1995) and Coziol (1996), one piece of evidence in favour of a sequence of bursts was the predominance of B-type stars in starburst nucleus galaxies. We can repeat the analysis performed in Coziol (1996) to verify this result in the NIR. The advantage of working in the NIR is that the extinction in this part of the spectrum is less severe, and the fraction of obscured stars should therefore be less important (Calzetti et al. 1995), decreasing the uncertainties related to this method.

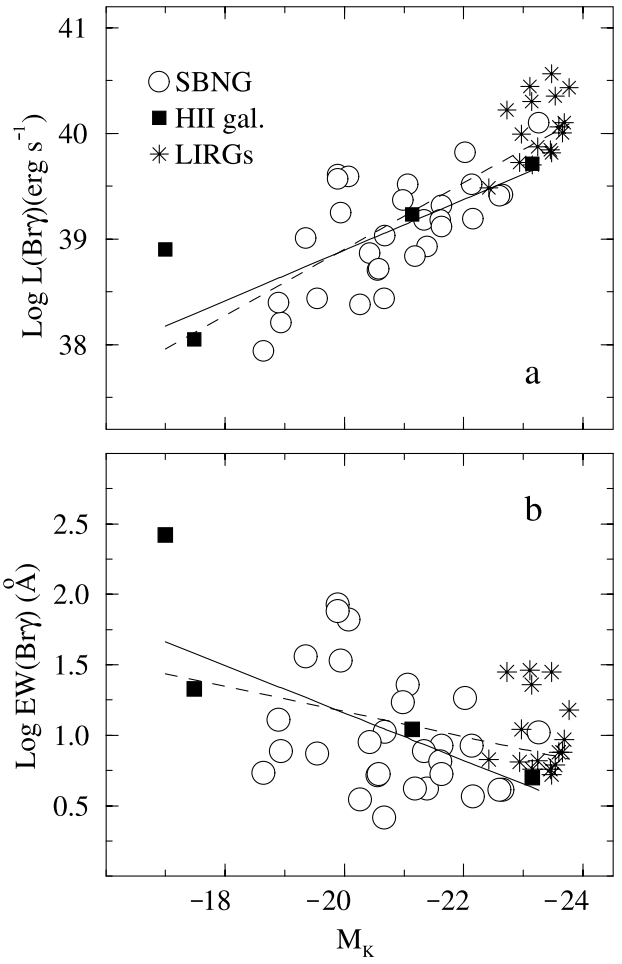

Figure 9. Relation between Brγ and absolute K magnitude. The continuous curves in (a) and (b) are linear regressions obtained using only our galaxies. The dashed curves are linear regressions obtained after adding the LIRGs to our galaxies. The coefficients of correlation are given in the text. The two dashed curves in (a) and (b) are linear regressions obtained after adding the LIRGs to our sample of galaxies.

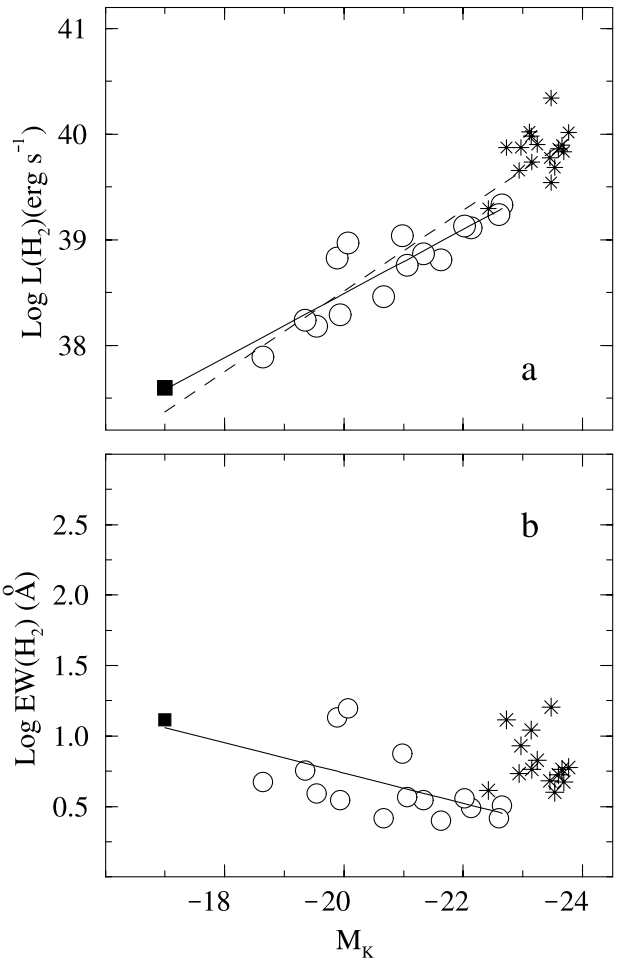

Figure 10. Relation between H_2 and K-band absolute magnitude. The symbols and curves have the same meaning as in Fig. 9.

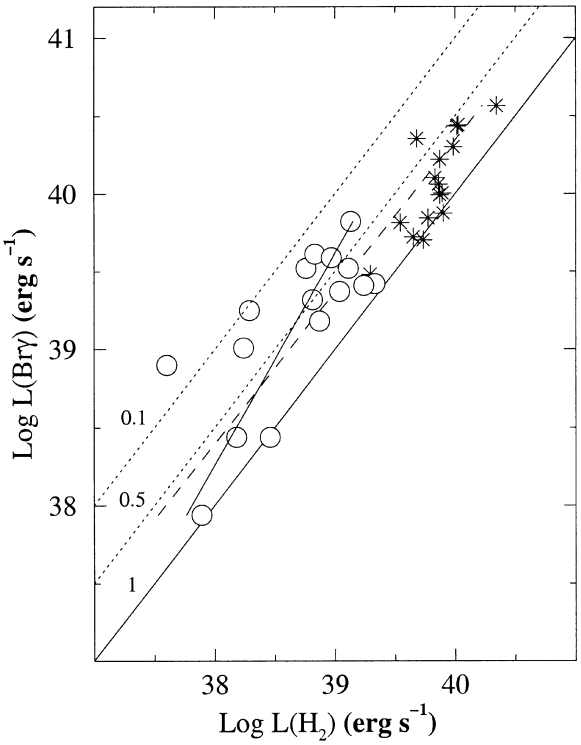

Figure 11. Relations between Brγ and H_2 luminosities. The symbols have the same meaning as in Fig. 9. The diagonal lines correspond to the luminosity ratios 1.0, 0.5 and 0.1, consistent with values predicted by shocks or fluorescence models. The short continuous curve is a linear regression on our sample of galaxies. The dashed curve is a linear regression obtained after adding the LIRGs to our sample of galaxies.

The level of extinction in our galaxies can be estimated (Fig. 12a) by comparing L(Brγ) with the luminosity in Hα [L(Hα)]. Using a photoionization model, one can deduce a 'theoretical' relation between L(Brγ) and L(Hα). The theoretical relation deduced by Leitherer & Heckman (1995) is shown in Fig. 12(a) as a continuous curve. The difference between this relation and observation is due to dust extinction, which affects Hα more the Brγ. The higher the extinction, the lower the L(Hα)/L(Brγ) ratios. In Fig. 12(a) the dashed curves correspond to ratios assuming dust extinction varying between 1 and 5 mag. From this figure, we deduce that the extinction in our galaxies varied between 0 and 2 mag, which is in good agreement with values estimated from the Balmer decrement method (Contini, Considère & Davoust 1998). The LIRGs on the other hand seem to suffer slightly higher dust extinction, the values varying between 3 and 4 mag.

Once corrected for extinction, the flux ratios Brγ/L_{IR} are proportional to the ionizing flux produced by stars with various spectral types (Devereux & Young 1990). In Fig. 12(b) we show the locus expected for ionizing star clusters with different spectral types. This figure confirms the dominance of B-type stars as found in Coziol (1996).

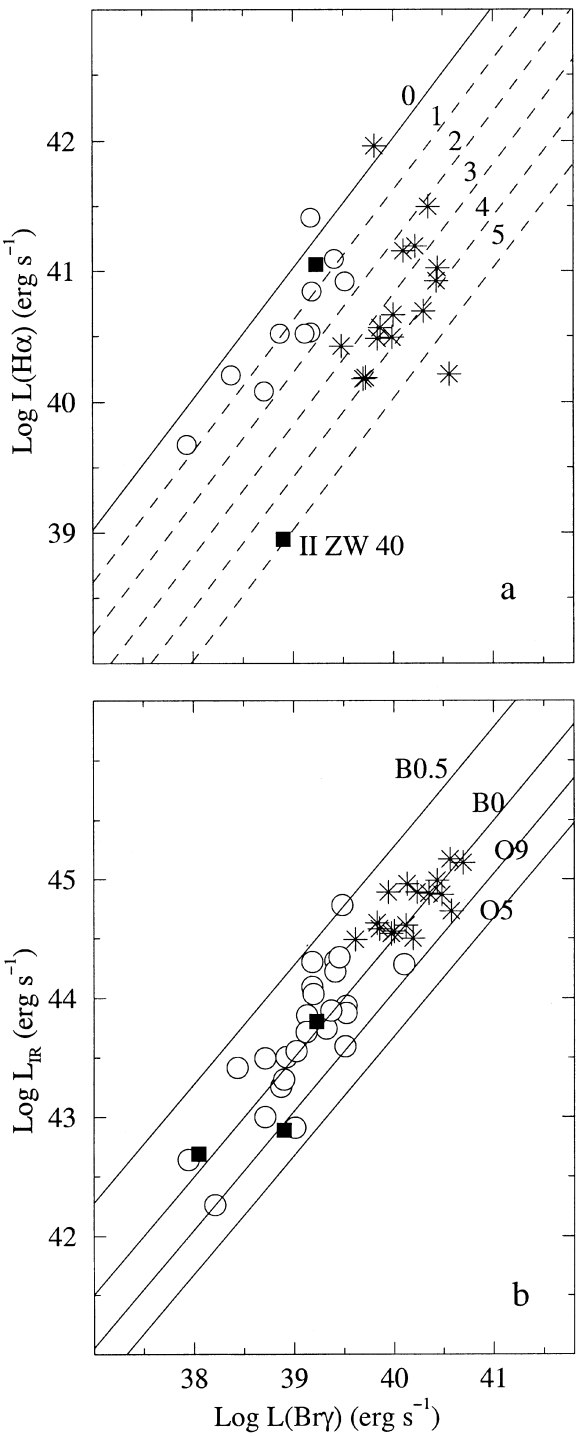

Figure 12. (a) The relation between Hα and Brγ luminosities. The different diagonal lines correspond to theoretical ratios between the luminosities, assuming various magnitudes of extinction as indicated by the numbers. (b) The relation between the FIR and Brγ luminosities. The diagonal lines are theoretical ratios expected for different spectra types. The luminosities of Brγ were corrected for extinction as determined in panel (a).

5 DISCUSSION

The question that we need to answer is this: can we accept the result of the synthetic starburst model? In order to answer this question we first need to better understand this result. The main reason why the instantaneous burst solution is rejected by our observation is because the predictions of the models are in contradiction with the values of the CO spectral indices we measured. In an instantaneous burst, the Brγ equivalent width stays high for the first 10^7 yr. During this time, CO_{spec} is negligible and begins to increase only at around 10^7 yr, when the most massive stars evolve as RSGs. It is because we observe both intense Brγ emission and relatively strong CO lines that we need continuous

star formation. The answer seems, therefore, to rely on the validity of the CO spectral index.

To obtain a good fit with any of the instantaneous burst models, the CO spectral indices would need to decrease by more than 50 per cent. Obviously, this cannot be a result of the method we used to measure these lines. The strength of the CO bands in our spectra is undeniable. A relatively strong value of CO_{spec} is consistent with a predominance of RSGs over RGs (Doyon et al. 1994). This is consistent with the correlation found between M_K and $L(\mathrm{Br}\gamma)$, which suggests that the stars producing this luminosity, and probably also the CO band, are related to the burst population. Moreover, this relation is relatively weak because RSGs only appear in greater numbers shortly after the culmination of the burst. The relatively strong CO bands in our spectra seems therefore to be real, and a constant star formation rate is consequently necessary to explain our data.

However, what about the low upper mass cut-off? If we look at Fig. 5, we see that the reason why we need such a feature is because the Brγ equivalent widths seem too weak as compared to the model with upper mass cut-off $M_{\mathrm{up}} = 100\,\mathrm{M}_{\odot}$. Now, this result is far from obvious. It is therefore highly significant that when we determine the spectral types of the ionizing stars in these galaxies we find a value which is consistent with this result: the dominant ionizing stars are early-type B or late-type O, which have masses of the order of 10 to $20\,\mathrm{M}_{\odot}$ (Panagia 1973), in good agreement with the upper mass cut-off suggested by the model. We have therefore concluded that the solution suggested by the synthetic starburst model is fully consistent with our data.

Then how could star formation be continuous? In order to sustain star formation in starburst galaxies, some mechanism other than interaction is necessary. Observations of nearby starburst galaxies suggests that most ($\sim$70 per cent) of these galaxies are relatively isolated and cannot be associated to ongoing interaction events (Telles & Terlevich 1995; Coziol et al. 1997). In our sample, only five galaxies have a peculiar morphology, suggesting some sort of direct interaction. The best example is NGC 1089. The galaxy II Zw 40, on the other hand, which also has the youngest burst, cannot be easily connected to an interaction event. The same is true for most of the galaxies in our sample. More than two thirds of our sample galaxies are isolated early-type spirals (earlier than Sbc: a total of 19 galaxies) or galaxies with a compact appearance (14 galaxies). The rest (10 galaxies) looks like normal late-type spirals (Sbc or later). There is, consequently, no obvious dynamical cause for the bursts observed in most of these galaxies, which suggests that some 'internal' regulating or self-sustained star formation mechanism must be active.

In order for star formation to be continuous over a significantly long period of time, star formation rates cannot be very high either. This may be in contradiction with some observations of very intense starburst galaxies. This is why a sequence of bursts may be a more interesting alternative. If the bursts are intense but do not last very long, the reservoir of gas will not be exhausted, allowing ignition of new bursts later on. Assuming some self-regulated mechanism, this process could probably extend over a relatively long period of time. One can already find in the literature different mechanisms capable of producing bursts in sequence, either by regulation or propagation of star formation from supernovae feedback (Gerola, Seiden & Schulman 1980; Krügel & Tutukov 1993) or multiple small-merger events on a few-Gyr period (Tinsley & Larson 1979). These two alternatives were already found to be consistent with the chemical properties of nearby starburst galaxies (see Coziol et al. 1997 and 1999 for example).

What evidence do we have in favour of a sequence of bursts? In our spectra we have found some variation of burst characteristics with the aperture, which suggests that the bursts are not homogeneous in space. The fact that we do not observe systematic trends for these variations suggests that their origin may be related to the particular star formation history of each galaxy. This could be one signature of internal processes. Considering that these variations are observed over regions a few kpc wide, it is probably also more realistic to assume that different star formation events occurred during different time intervals (this would be the case for star formation propagation). The dispersion of the *K*-band absolute magnitude versus (Brγ) equivalent width relation is highly suggestive of some intermittent events, superimposed, perhaps, on a more global behaviour.

However, the strongest evidence in favour of a sequence of bursts may be the predominance of early-type B stars in the ionized regions of these galaxies. Such stars, with masses of the order of 10 to $20\,\mathrm{M}_{\odot}$, have lifetimes of only a few 10^7 yr. For one burst population, it is therefore difficult to understand how this particular composition of stars is possible. This cannot be explained solely in terms of an age effect. Indeed, the main sequence lifetime of these stars is only a factor of 10 older than those of more massive stars and a factor of 10 younger than the age of the bursts deduced from the synthetic starburst model, which would mean that we observe all these galaxies in a very particular and short phase of their evolution. Considering the generality of our observations, this makes it a very improbable event.[2]

A sequence of short bursts, on the other hand, without any limit on the upper mass cut-off and extending over a relatively long period of time (a few 10^8 yr or 1 Gyr) in order to mimic continuous star formation, may reproduce such phenomenon. Short bursts would produce few massive stars, which would then evolve rapidly and all disappear before another burst began. Depending on the frequency of the bursts, the average population would then evolve statistically towards the predominance of early-type B stars. Note that it is probably impossible to reproduce such stellar populations with constant star formation, unless the IMF upper mass cut-off is truncated towards low-mass stars.

To finish, we have concluded that we cannot identify what the mechanism responsible for the H_2 emission in our galaxies is. However, the different time-scales over which these processes culminate should help us estimate which mechanism is the more probable one. Supernovae shock remnants are predominant only when a high number of massive stars are produced and the bursts are very young (a few 10^4 yr). Infrared fluorescence, on the other hand, is produced by early B stars, which radiate ample photons in the Lyman–Werner band ($\lambda = 912$–1108Å). These stars have longer lifetimes and should therefore prevail only when the burst is old or, for some reason, the stars are predominant in a burst population. The fact that B stars do seem to be over-abundant in our galaxies suggests that fluorescence must be the main mechanism responsible for the H_2 emission. One would then expect to see an increase of fluorescent emission in regions where B stars dominate over O stars (Tanaka, Hasegawa & Gatley 1991). This would explain some of the variations we observed when we change the aperture, which would consequently produce another piece of evidence in favour of the multiple bursts scenario hypothesis.

[2]It is doubtful that we can explain such rare events based on the obvious bias that these are starburst galaxies, considering that such galaxies form between 25 to 30 per cent of all the galaxies in the nearby Universe.

6 CONCLUSION

Although the solution proposed by the application of the synthetic starburst models to our sample of starburst galaxies may look counter-intuitive, we have shown that it seems to be fully consistent with our data. Our analysis confirms, therefore, the results previously obtained by Deutsch & Willner 1986, Doyon, Puxley & Joseph (1992), Coziol & Demers 1995, Coziol (1996) and Goldader et al. (1997b).

However, the solution proposed by the models may not represent strong constraints on the duration of the burst or the form of the IMF. This is because the models cannot distinguish between constant star formation or a sequence of short bursts over an extended period of time. This alternative, the sequence of short bursts, will have to be tested fully before we can conclude on the values of these two important parameters in starburst galaxies.

Whatever the solution is, our observations are clear on one thing, which is that starburst must be a sustained or self-sustained phenomenon: either star formation is continuous in time or different bursts happen in sequence over a relatively long period of time. The generality of our observations suggests that this is a characteristic of starburst galaxies in the nearby Universe.

ACKNOWLEDGMENTS

RC would like to thank the Observatoire de Besançon for supporting his work. The authors would also like to thank Leitherer et al. for making their synthetic starburst models available to the community and an anonymous referee for interesting comments and useful suggestions. This research has made use of the NASA/IPAC Extragalactic Database (NED) which is operated by the Jet Propulsion Laboratory, Caltech, under contract with the National Aeronautics and Space Administration.

REFERENCES

Alonso-Herrero A., Engelbracht C. W., Rieke M. J., Rieke G. H., Quillen A. C., 2001, ApJ, 546, 952
Anantharamaiah K. R., Viallefond F., Mohan N. R., Goss W. M., Zhao J. H., 2000, ApJ, 537, 613
Augarde R., Chalabaev A., Comte G., Kunth D., Maehara H., 1994, A&AS, 104, 259
Allen M. L., Kronberg P. P., 1998, ApJ, 502, 218
Baldwin J. A., Phillips M. M., Terlevich R., 1981, PASP, 93, 5
Balzano V. A., 1983, ApJ, 268, 602
Calzetti D., Bohlin R. C., Kinney A. L., Storchi-Bergman T., Heckman T. M., 1995, ApJ, 443, 136
Contini T., Considère S., Davoust E., 1998, A&AS, 130, 285
Coziol R., 1996, A&A, 309, 345
Coziol R., Demers S., 1995, Astrophys. Lett. Commun., 31, 41
Coziol R., Demers S., Peña M., Torres-Peimbert S., Fontaine G., Wesemael F., Lamontagne R., 1993, AJ, 105, 35
Coziol R., Demers S., Peña M., Barnéoud R., 1994, AJ, 108, 405
Coziol R., Demers S., Barnéoud R., Peña M., 1997, AJ, 113, 1548
Coziol R., Torres C. A. O., Quast G. R., Contini T., Davoust E., 1998, ApJS, 119, 239
Coziol R., Carlos-Reyes R. E., Consière S., Davoust E., Contini T., 1999, A&A, 345, 733
de Grijs R., O'Connell R. W., Gallagher J. S., III, 2001, AJ, 121, 768
Deutsch L. K., Willner S. P., 1986, ApJ, 306, L11
Devereux N. A., Young J. S., 1990, ApJ, 350, L25
Doyon R., Puxley P. J., Joseph R. D., 1992, ApJ, 397, 117
Doyon R., Joseph R. D., Wright G. S., 1994, ApJ, 421, 101
Doyon R., Nadeau D., Joseph R. D., Goldader J. D., Sanders D. B., Rowlands N., 1995, ApJ, 450, 111
Elmegreen B., 1999, in Livio M. ed., Unsolved Problems in Stellar Evolution. Cambridge Univ. Press, Cambridge in press (astro-ph/9811289)
Gerola H., Seiden P. E., Schulman L. S., 1980, ApJ, 242, 517
Goldader J. D., Joseph R. D., Doyon R., Sanders D. B., 1995, ApJ, 444, 97
Goldader J. D., Joseph R. D., Doyon R., Sanders D. B., 1997a, ApJ, 474, 104
Goldader J. D., Joseph R. D., Doyon R., Sanders D. B., 1997b, ApJS, 108, 449
Goudfrooij P., Mack J., Kissler-Patig M., Meylan G., Minniti D., 2001, MNRAS, 322, 643
Hunter D. A., O'Connell R. W., Gallagher J. S., Smecker-Hane T. A., 2000, AJ, 120, 2383
Kaaret P., Prestwich A. H., Zezas A., Murray S. S., Kim D.-W., Kilgard R. E., Schlegel E. M., Ward M. J., 2001, MNRAS, 321, L29
Kennicutt R. C., Jr., 1983, ApJ, 272, 54
Kim D.-C., Sanders D. B., Veilleux S., Mazzarella J. M., Soifer B. T., 1995, ApJS, 98, 129
Krügel E., Tutukov A. V., 1993, A&A, 275, 416
Leitherer C., Heckman T. M., 1995, ApJS, 96, 9
Leitherer C. et al., 1999, ApJS, 123, 3
Liu C. T., Kennicutt R. C., 1995, ApJS, 100, 325
Londsdale C. J., Helou G., Good J. C., Rice W., 1985, Catalogued Galaxies and Quasars Observed in the *IRAS* Survey, JPL D-1932. Jet Propulsion Laboratory, Pasadena
Izotov Y. I., Thuan T. X., Lipovetsky V. A., 1998, ApJ, 497, 227
Masegosa J., Moles M., Campos-Aguilar A., 1994, ApJ, 420, 576
Mas-Hesse J. M., Kunth D., 1999, A&A, 349, 765
Mayya Y. D., 1997, ApJ, 482, L149
Mazzarella J. M., Boroson T. A., 1993, ApJS, 85, 27
Meurer G. R., 2000, in Lançon A., Boily C. M. eds, ASP Conf. Ser. Vol. 211, Massive Stellar Clusters. Astron. Soc. Pac., San Francisco, p. 81
Moorwood A. F. M., Oliva E., 1990, A&A, 239, 78
Mountain C. M., Robertson D. J., Lee T. J., Wade R., 1990, in Instrumentation in Astronomy VII, Soc. Photo-Optical Instr. Eng., Bellingham, p. 14
Panagia N., 1973, ApJ, 78, 929
Pugh E. M., Winslow G. H., 1966, The Analysis of Physical Measurements. Addison-Wesley, Section 12-8
Puxley P. J., Hawarden T. G., Mountain C. M., 1990, ApJ, 364, 77
Puxley P. J., Doyon R., Ward M. J., 1997, ApJ, 476, 120
Raimann D., Bica E., Storchi-Bergmann T., Melnick J., Schmitt H., 2000, MNRAS, 314, 295
Rieke G. H., Lebofsky M. J., 1986, ApJ, 304, 326
Rieke G. H., Loken K., Rieke M. J., Tamblyn P., 1993, ApJ, 12, 99
Salzer J. J., MacAlpine G. M., Boroson T. A., 1989, ApJS, 70, 447
Saunders W., Rowan-Robison M., Lawrence A., Efstathiou G., Kaiser N., Ellis R. S., Frenk C. S., 1990, MNRAS, 242, 318
Schaerer D., Guseva N. G., Izotov Y. I., Thuan T. X., 2000, A&A, 362, 53
Schinnerer E., Eckart A., Boller Th., 2000, ApJ, 545, 20
Seaquist E. R., Frayer D. T., Frail D. A., 1997, ApJ, 487, 131
Sekiguchi K., 1987, ApJ, 316, 145
Tanaka M., Hasegawa T., Gatley I., 1991, ApJ, 374, 516
Telles E., Terlevich R. J., 1995, MNRAS, 275, 1
Terlevich R., Melnick J., Masegosa J., Moles M., Copetti M. V. F., 1991, A&A, 91, 285
Tinsley B. M., Larson R. B., 1979, MNRAS, 186, 503
Vader J. P., Simon M., 1987, AJ, 94, 854
Vacca W. D., Conti P. S., 1992, ApJ, 410, 543
Veilleux S., Osterbrock D. E., 1987, ApJS, 63, 295
Veilleux S., Kim D.-C., Sanders D. B., 1999, ApJ, 522, 113

This paper has been typeset from a TEX/LATEX file prepared by the author.